Egypt.J.Chem. **Vol. 62**, No. 10. pp. 1823 - 1849 (2019)

Egyptian Journal of Chemistry
http://ejchem.journals.ekb.eg/

A New Modified Exfoliated Graphene Oxide for Removal of Copper(II), Lead(II) and Nickel(II) Ions from Aqueous Solutions

A. F. Shaaban[1], A. A. Khalil[1], B. S. Elewa[2*], M. N. Ismail[3], U. M. Eldemerdash[2]
[1]*Chemistry Department, Faculty of Science, Benha University, Benha, Egypt.*
[2]*Department of Basic Engineering Sciences, Benha Faculty of Engineering, Benha University, Egypt.*
[3]*Polymers & Pigments Department, National Research Centre, Dokki, Giza, Egypt.*

AN effective and facial method for removal of lead(II), copper(II) and Nickel(II) ions from aqueous solutions, is based on investigating a new modified graphene oxide, by appealing interaction between graphene oxide GO and 4-amino-2,3-dimethyl-1-phenyl-3-pyrazolin-5-one(4-aminoantipyrine). The adsorbent is fully characterized by FT-IR, XRD, SEM, EDX, TEM, and Raman spectroscopy. The GO was prepared using a modified Hummers method by the reaction of potassium permanganate with graphite in presence of a mixture of sulfuric and phosphoric acids. This novel solid phase adsorbent 4-aminoantipyrine-GO was utilized to adsorb Pb(II), Cu(II) and Ni(II) ions from aqueous solutions because of amide functional group, is resulting an efficient adsorption. Also the abundant oxygen-containing functional groups on the surfaces of graphene oxide GO play an important role in metal ions sorption. The adsorption isotherms data were well fitted with Langmuir isotherm for Pb(II), Cu(II) and Freundlich isotherm for Ni(II) ions respectively. The kinetics of Pb(II), Cu(II) and Ni(II) ions adsorption were well fitted with pseudo second-order equation. The results of thermodynamic parameters referred to chemical adsorption. Also the positive values of standard heat of adsorption (ΔH^o) and negative values of (ΔG^o) indicated that the adsorption process was endothermic and spontaneous.

Keywords: Graphene oxide, 4-Aminoantipyrine, Metal ions, Isotherms, Kinetics, Thermodynamics, Regeneration.

Introduction

Water contamination by many pollutants such as textile dye, heavy metals and pharmaceuticals globally are creating major risks to the public health and the environment [1]. The pollution with the heavy metals has a poisonous effect on organisms even at trace levels. Additionally, it results in a serious disease such as cancer, anemia, and intellectual disability [2,3]. Heavy metals removal from aqueous environment has been investigated through chemical precipitation, ion exchange, membrane separation, adsorption, and coagulation [4–7]. Most of these methods have some limitations and disadvantages [8]. For example, precipitation is inefficient because it produces large quantities of sludge that require careful management. However, electrochemical treatment requires relatively high operating costs [9]. Between different approaches, adsorption is the most extensively used method due to its simplicity, flexibility, insensitivity to toxic substances, high efficiency in large scale applications and low cost [10–14]. Traditional adsorbents such as activated carbon, clay, chitosan, magnetic sorbents [15], resins [16-18], silica [19,20], zeolites, metal oxides and alginate suffer from poor adsorption sites, low selectivity and poor regeneration which limit their practical applications real processes. Therefore, it would be valuable to enhance the performance of traditional adsorbents by introducing new specific functional groups through chemical modification [21]. Graphene oxide, as two-dimensional carbon-

*Corresponding author e-mail: boosys36@gmail.com
Received 24/3/2019; Accepted 9/4/2019
DOI: 10.21608/ejchem.2019.11060.1713

based substance, has attractive properties because it has high mechanical strength (more than 1060 GPa), large specific surface area (nearly 2600 m^2/g), and riching in oxygenous functional groups (carboxyl, epoxy, and hydroxyl groups) [22–25]. GO is an efficient adsorbent for heavy metal ions [26–29], humic acid [30], radionuclides [31–34], organic dyes [35,36], ammonia [37]. due to its good dispersion in water, biocompatibility, and relatively easy and cost effective preparation methods [38,39]. Therefore, functionalization of GO with molecules containing strong chelating groups such as nitrogen and thiol can significantly enhance its removal efficiency [40–43].

The present work aims to: (I) preparing of GO nano sheets by improved hummers method from graphite; (II) preparing of acyl-chloride of graphene oxide nano sheets GO-Cl; (III) functionalization of 4-aminoantipyrine onto GO-Cl for adsorption of Pb(II), Cu(II) and Ni(II) ions from aqueous solutions; (IV) Characterization of all the above synthesized substances by FT-IR, XRD, SEM with EDX, TEM, and Raman spectroscopy; (V) A study of Langmuir and Freundlich adsorption isotherms also the adsorption kinetics and thermodynamic parameters of Pb(II), Cu(II) and Ni(II) ions adsorption from aqueous solutions onto the new functionalized graphene oxide 4-aminoantipyrine-GO; (VI)Regeneration and recycling studies of loaded 4-aminoantipyrine -GO.

Experimental

Materials

Graphite powder and 4-aminoantipyrine of high purity was supplied by sigma Aldrich. The improved hummers oxidizing mixture was consisted of concentrated sulfuric and phosphoric acids H_2SO_4 & H_3PO_4 and potassium pomegranate $KMnO_4$ also were supplied by sigma Aldrich. Chemicals reagents of 30% hydrogenperoxid H_2O_2, thionylchloride $SOCl_2$, triethylamine TEA, sodium hydroxide NaOH and dimethylformamide DMF was supplied by sigma Aldrich. Hydrochloric acid HCl, nitric acid HNO_3, terahydrofuran THF and ethanol were used for washing purpose. All solvents were used as its without any purification. The sources of metal ions are coppersulphatepentahydrate $CuSO_4.5H_2O$, lead acetatetrihydrate $Pb(CH_3COO)_2.\ 3H_2O$ and nickelchloridehexahydrate $NiCl_2.6H_2O$ salts which were supplied by sigma Aldrich. EDTA, buffer solution (pH=10), EriochromeBlackT and murioxide were used for titration experiments. Deionized water from local source was used when needed.

Methods

Preparation of GO nano sheets from graphite by modified hummers method[44]

A modified method was used for the synthesizing of GO. A (20: 180) mixture of concentratedH_3PO_4–$H_2SO_4$to a mixture of graphite flakes 1.5 g and $KMnO_4$ 9.0 g. The reaction was slightly exothermic at a temperature range of (35–40) ^oC, after which it was heated up to 50 ^oC with continuous stirring for 12 h. Then the reaction mixture was cooled to room temperature and slowly poured onto 200 ml ice with 2 ml of 30%H_2O_2 where the brown color was entirely turned to yellow. The mixture was then centrifuged at 5000 rpm and the remaining solid material was washed with 200 ml of water, 200 ml of 30% HCl, and 200 ml of 2% ethanol. The produced GO was then subjected to vacuum drying at room temperature for 24 hours.

Preparation of acyl-chloride of graphene oxide nano sheets (GO-Cl) [44]

0.5 g of GO was dispersed in 10 ml dimethylformamide DMF then treated with 50 ml of a thionylchloride $SOCl_2$. The resulting mixture was refluxed at 70 ^oC for 48 hours and then centrifuged several times at 5000 rpm for 45 min to isolate the precipitate. The precipitate was washed several times with tetrahydrofuran THF and dried under vacuum.

functionalization of (4-aminoantipyrine) onto (GO-Cl) to produce (4-aminoantipyrine -GO) nanosheets

In the presence of triethylamine 2 ml, the GO-Cl 0.5 g was dispersed in DMF 20 ml, then was allowed to react with 4-aminoantipyrine 0.5 g. the reaction was refluxed at 70 ^oC for 72 hours. After that, the solution was cooled to room temperature and centrifuged. Then the precipitate 4-aminoantipyrine -GO was washed with THF for several times and then dried at room temperature for 24 h under vacuum.

Adsorption experiments

The adsorption experiments were conducted using batch technique. Batch adsorption isotherms studies were investigated using different concentrations of Pb(II), Cu(II) and Ni(II) ions solutions. 0.01 g of the 4-aminoantipyrine -GO adsorbent were taken for analysis in an aqueous phase volume of 25 ml of Pb(II), Cu(II) and Ni(II) ions. At optimum pH (5.35, 5.5&5.9) for Pb(II),

Cu(II) and Ni(II) ions respectively. The pH of the adsorptive solutions was adjusted with the suitable quantity of diluted NaOH and HCl, monitored with a digital pH meter. The concentration of supernatant solutions was determined by titration with (0.01M EDTA) in the presence of suitable indicator; EriochromeBlackT for Pb(II) ion and Murioxide for Cu(II) and Ni(II) ions. The amount of metal ion adsorbed per unit mass of adsorbent and the percentage of removal were calculated using equations 1 and 2[82].

$$q_e = (C_o - C_e)(V/m) \quad (1)$$

$$\%\,\text{Removal} = 100 * (C_o - C_e)/C_o \quad (2)$$

Where q_e is the adsorption capacity (mmol/g), C_o and C_e are the initial and equilibrium metal ion concentration (mmol/L) in the aliquots, respectively. V (ml) is the solution volume and m (g) is the mass of sorbent.

Characterization

The methods were used for characterization of the synthesized samples: FT-IR spectroscopy using FT/IR-BRUKER, Vector 22 (Germany) Spectrophotometer, XRD using Bruker company model D8, SEM/EDX microscopy using the Bruker X-Flash 410 detector supplied with Energy dispersive X-ray micro analysis system, TEM using the Jeol JEM-1230 microscope, and Raman spectroscopy using the Thermo Scientific DXR Smart Raman with three different laser source 325 nm, 532 nm and 785nm.

The current adsorbent system is based on the introduction of nitrogen chelating groups within chemically functionalized GO as shown in Scheme 1. The GO was produced by oxidation of graphite using modified Hummers methods (H_2SO_4/ H_3PO_4/ $KMnO_4$) according the reported method [44]. GO was first modified with $SOCl_2$ to convert the carboxyl and some of hydroxyl groups into acyl chloride groups which can react with 4-aminoantipyrine chelating groups. Since 4-aminoantipyrine functional groups could supply NH chelating groups, for the removal of Lead, Copper and Nickel ions from its aqueous solutions.

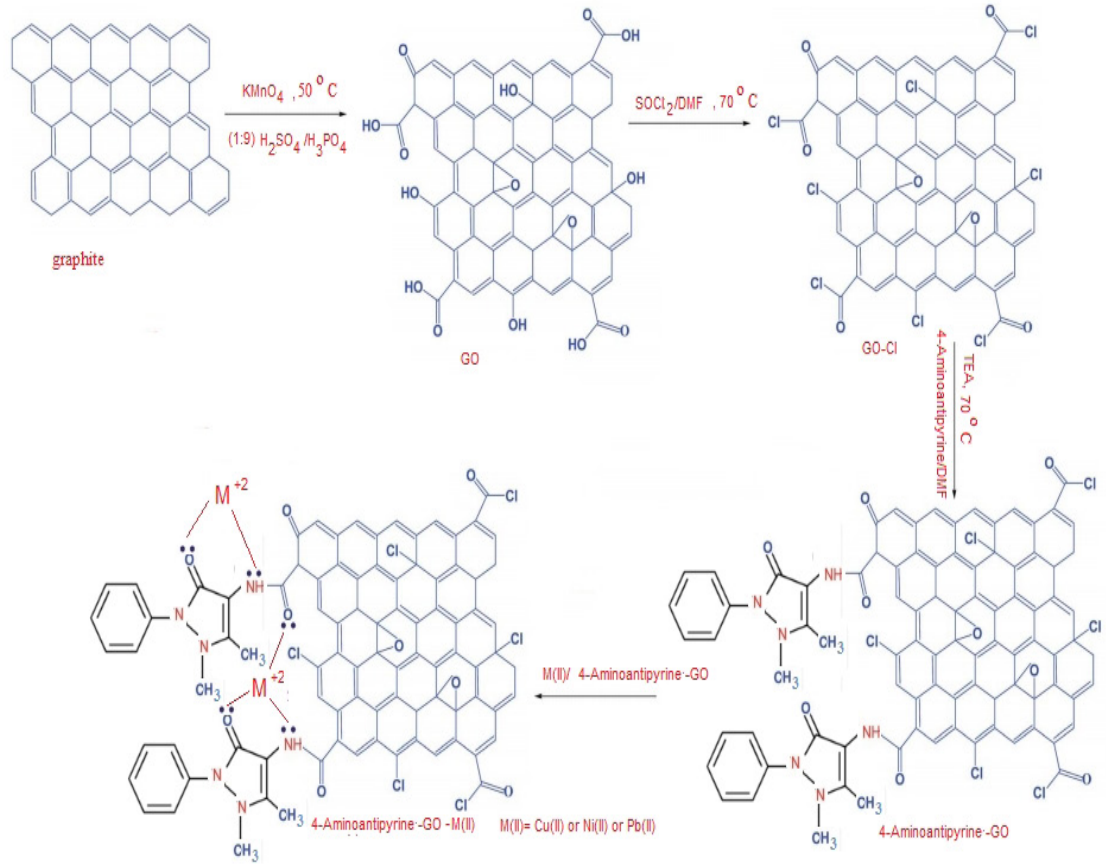

Scheme 1. presentation of the steps of modification of GO & the complexation with the Pb(II), Cu(II) and Ni(II) ions.

FT-IR spectroscopy

FTIR analysis can be one of the direct evidence for the prepared samples GO, GO-Cl, 4-aminoantipyrine-GO as it provides information about the functional groups that present in the sample. The spectrum of GO (Fig. 1a) shows typical peaks of broad band at ~ 3200 cm^{-1} related to the O-H (free and carboxylic), while 1730 cm^{-1} corresponded to C=O stretching vibrations in the carboxylic acid groups, the peak at 1623 cm^{-1} is due to C=C in aromatic ring and 1176.28, 1056.5 and 849.35 cm^{-1} are for C–O–C stretching, symmetric, and asymmetric stretching vibrations in the epoxy groups, respectively at the GO surface [45-47]. Following the addition of thionyl chloride, the spectrum of the GO-Cl (Fig. 1b) illustrates absorption peaks at ~3445, 1703 and (1468, 601) cm^{-1} assigned to free hydroxyl groups, C=O stretching of the Cl-CO groups and the stretching vibrations of the C-Cl groups, respectively. Finally, the 4-aminoantipyrine -GO spectrum (Fig. 1c) shows peaks around 1680 and 1567 cm^{-1} attributed to the C=O stretching vibration and the N-H bending vibration of NHCO (amide) group, respectively.

Raman spectroscopy

Raman spectroscopy is employed to analyze the structural changes during chemical processing from graphene oxide to new functionalized graphene oxide. The Raman spectrum graphene oxide (Fig. 2a) shows the D-band at 1458.30 cm^{-1} and the G-band at 1600.64 cm^{-1}. It is well-known that the D-band reflected disorders and local defects, while the G-band related to the vibrations of SP^2 of carbon atoms in a graphitic 2D hexagonal lattice [48-50]. For GO, the D and G bands have equal intensity, indicating that graphite completely oxidized to GO. The ID/IG ratio is 0.94, confirmingless disorder and defect concentration and perfect aromatic structure in GO [51]. The Raman spectrum of 4-aminoantipyrine -GO (Fig. 2b) shows D-band at 1344.43 cm^{-1}, G-band at 1598.94 cm^{-1}, D` band at 2635 cm^{-1} and a 2D band at 2940 $cm^{-1}$are due to C=C SP^2 stretch vibration of olefnic/conjugated chains. The I(D)/I(G) ratio increased from 0.94 to 1.07 of 4-aminoantipyrine-GO due to increasing in the number of aromatic domains on the graphene oxide surface during the chemical functionalization [52]. 2D and 3D confocal images showed the shape of particles with different color (every color refer to one of chemical composition consist of materials) and its raman shift determine the chemical composition.

Powder X-Ray Diffraction Analysis (XRD)

The X-ray Diffraction patterns (XRD) of puregraphite (A0), GO (A1),GO-Cl (A2), 4-aminoantipyrine-GO (A3), 4-aminoantipyrine-GO-pb^{+2} (A4),4-aminoantipyrine-GO-Cu^{+2} (A5) and4-aminoantipyrine-GO-Ni^{+2} (A6) are shown in Fig. 3. The sharp peakof puregraphite at 2θ = 26.72 (d= 0.3331 nm) corresponding to the plane (002),thatshifts to 11.128 (d = 0.788 nm) on chemical oxidation, confirming the formation of GO. The C-axis spacing increases from 0.3331 to 0.788 nm by oxidation, due to the presence of oxygen-containing functional groups on the surfaces of GO [53]. This peak shifts to 2θ = 11.346 with an interlayer spacing of 0.779 nm in GO-Cl which may be due to the distortion of the crystal structure of GO. Finally the peak moves to 2θ = 11.026 and (d= 8.18nm) for 4-aminoantipyrine-GO. The large interlayer distance between the sheets due to the presence of 4-aminoantipyrine on the surface of the 4-aminoantipyrine-GO sheets through the amide linkages. New sharp peaks appear at 2θ = 30.911 & 39.19are characteristic for the complexes of pb^{+2}ions on 4-aminoantipyrine-GO surface. Also sharp peaks illustrates at 2θ =14.1, 21.9, 35.9, 39.19&62.1, which are characteristic for different types of Cu^{+2} complexes with 4-aminoantipyrine-GO surface, while the 4-aminoantipyrine-GO -Ni^{+2} complexes gave distinguishable peaks at 2θ =43.34, 44.3 & 63.with 4-aminoantipyrine-GO surface.

Scanning Electron Microscopy (SEM)

Surface morphologies of the GO and 4-aminoantipyrine-GO are determined by using SEM and the micrographs are shown on Fig. 4. GO (Fig. 4a) shows close wrinkled, aggregated, and thin sheets [54] compared to 4-aminoantipyrine-GO. While the binding of 4-aminoantipyrine to the carbon plane strongly effects on the morphology of 4-aminoantipyrine-GO (Fig. 4b). It can expand space between graphene sheets.

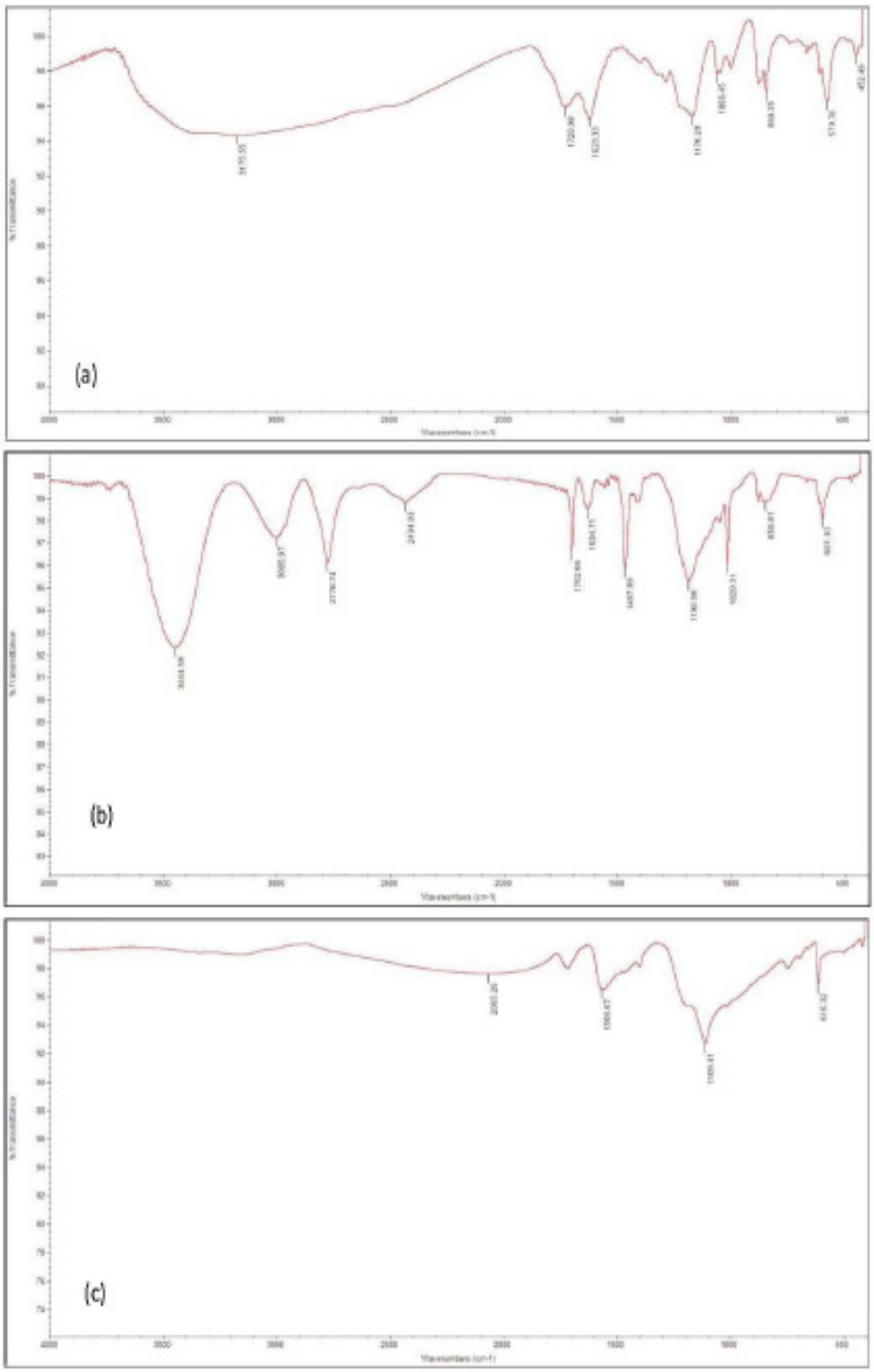

Fig. 1. FTIR Spectra of a) GO, b) GO-Cl & c) 4-aminoantipyrine -GO.

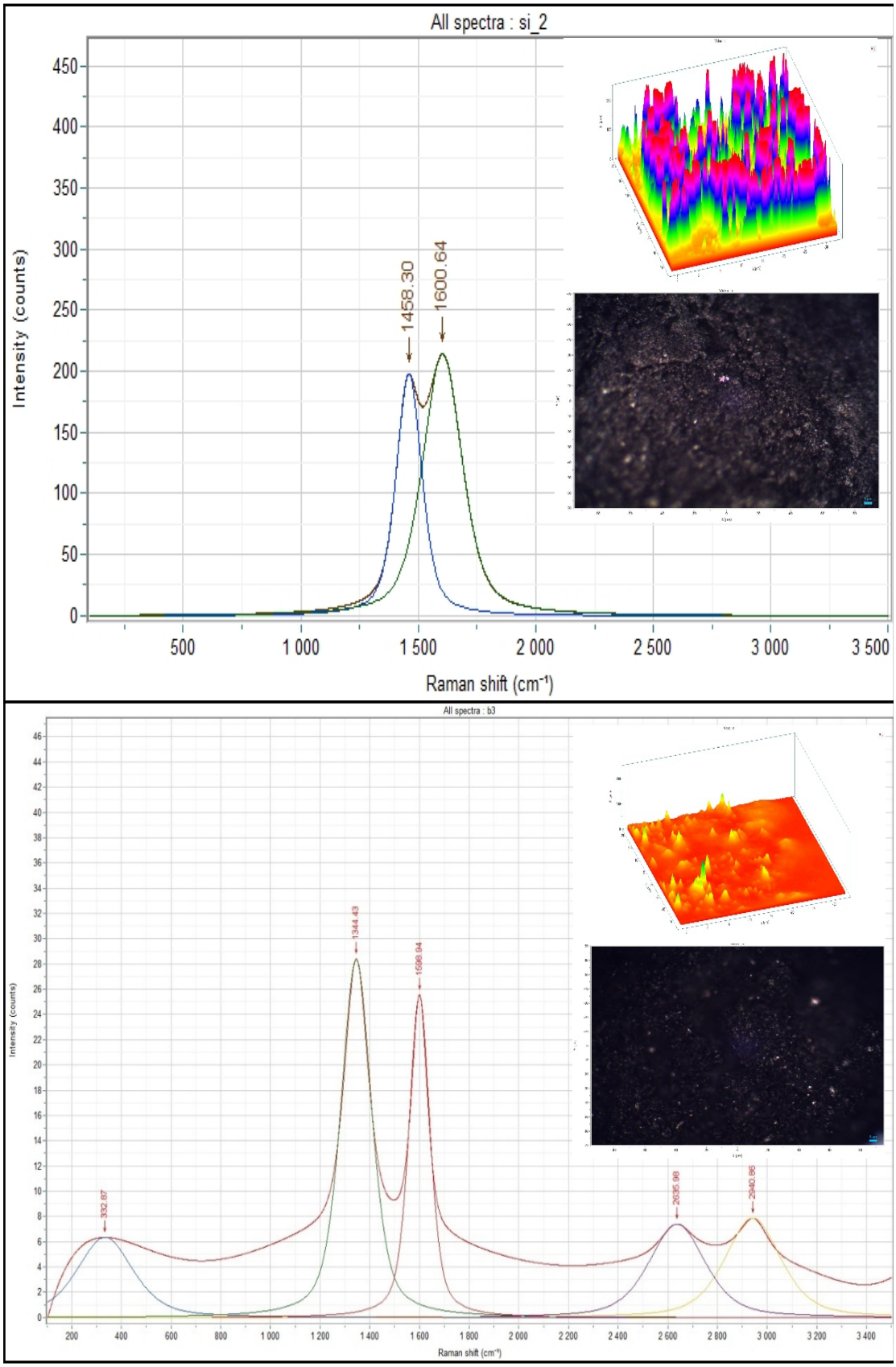

Fig. 2. Raman Spectra of a) GO & b) 4-aminoantipyrine -GO, with 2D and 3D confocal images.

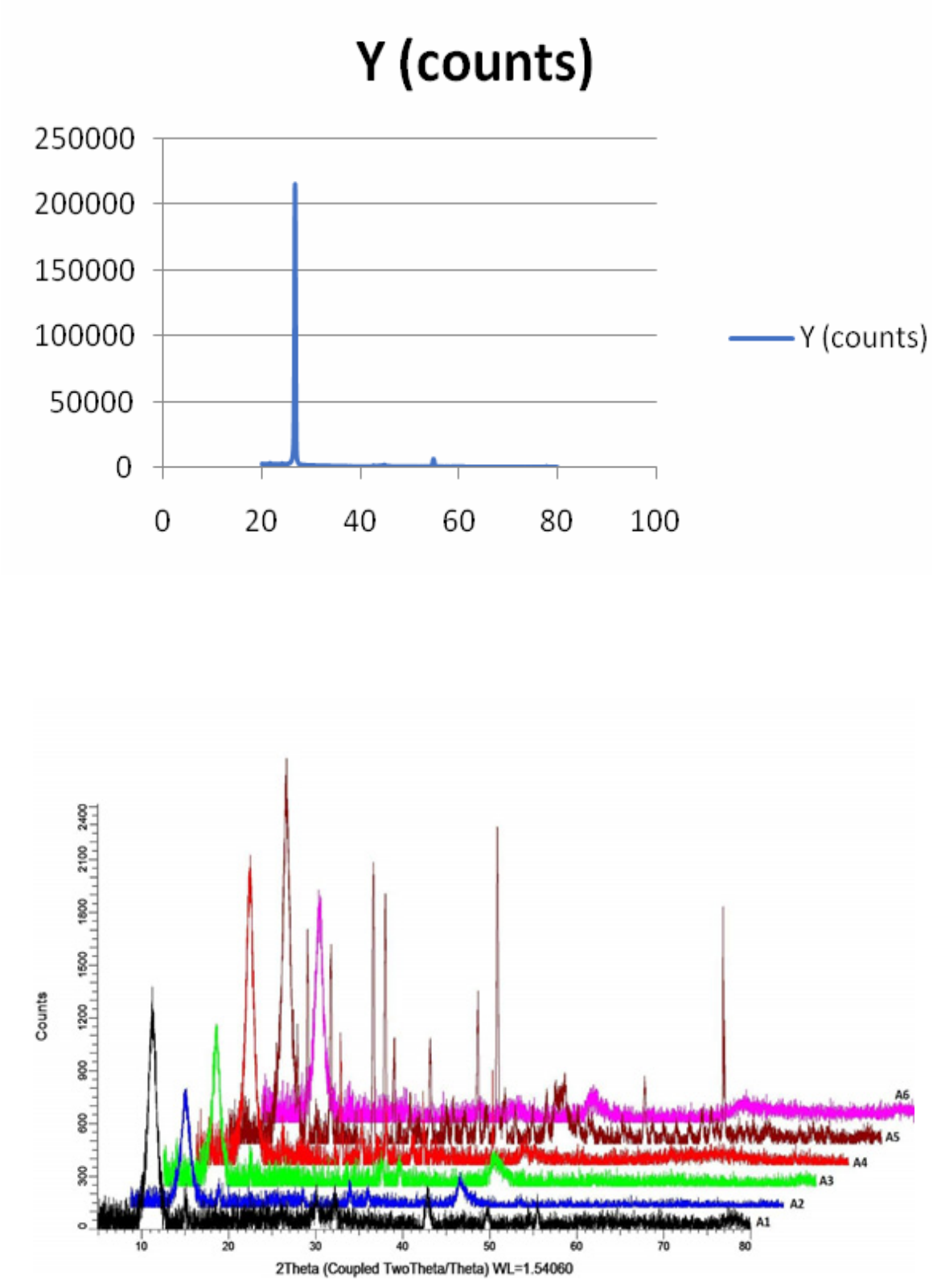

Fig. 3. XRD patterns of puregraphite (A0), GO (A1),GO-Cl (A2), 4-aminoantipyrine-GO (A3), 4-aminoantipyrine-GO-pb^{+2} (A4),4-aminoantipyrine-GO-Cu^{+2} (A5) &4-aminoantipyrine-GO-Ni^{+2} (A6).

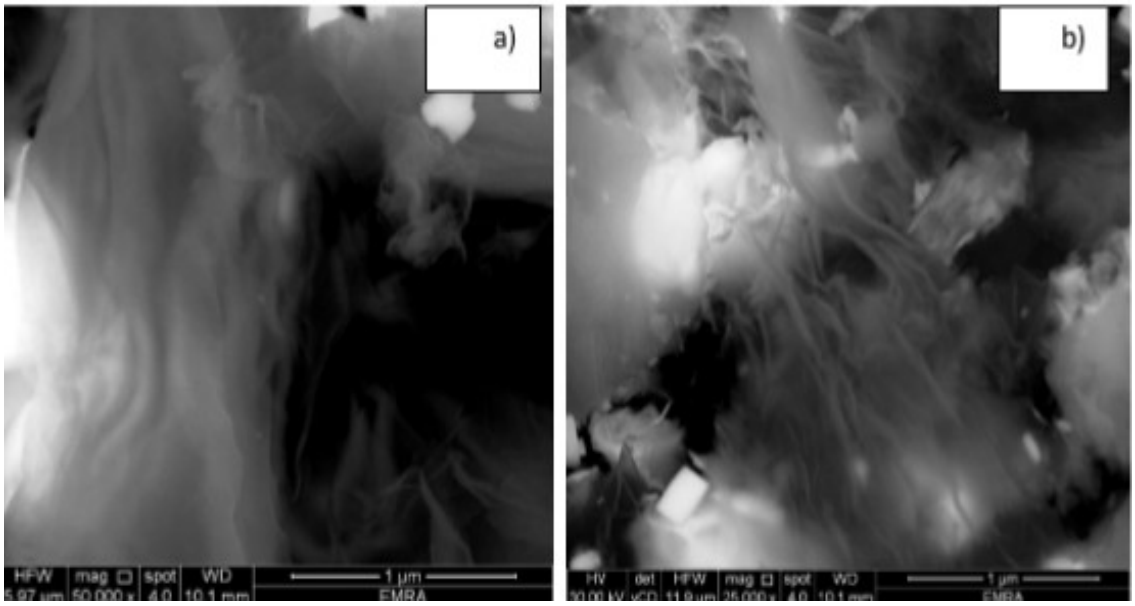

Fig. 4. SEM of a) GO & b) 4-aminoantipyrine-GO.

Energy-dispersive X-ray spectroscopy(EDX)

The composition of GO, 4-aminoantipyrine-GO and 4-aminoantipyrine-GO complexes with(pb^{+2},Cu^{+2} andNi^{+2}) ions were confirmed form Energy-dispersive X-ray spectroscopy (EDX). GO (Fig. 5a) shows distinct two signals at 0.27 and 0.52 keV for carbon and oxygen, respectively. After chemical modification (Fig. 5b), a new signal appears at 0.39 keV is distinguishable for nitrogen in 4-aminoantipyrine-GO. Finally after the metal ions adsorption experiments, Fig. 5c, 5d and 5e show distinct signals at (10.55 & 2.34), (0.9 & 8.1) and (7.47 & 8) keV , which are characteristic for lead , copper and nickel, respectively.

Transmission Electron Microscopy (TEM)

The second method for studying the Surface morphologies of the GO and 4-aminoantipyrine-GOis theTransmission Electron Microscopy (TEM). Figures 6a and 6b display the TEM images of GO and 4-aminoantipyrine-GO, indicates that the sheets of GO have smooth surfaces and appear to be thicker and slightly crumpled, while the chemically modified sheets of4-aminoantipyrine-GO which appear to have rougher and more wrinkled surface probably because of the covalent attachments of the oxygen and nitrogen containing functional groups.

Factors affecting the adsorption of Pb(II), Cu(II) and Ni(II) ions onto the 4-aminoantipyrine-GO adsorbent

Adsorbent dose

For the batch experiments, the amount of the adsorbent material was varied in the range of 0.01 to 0.05 g in a 25 ml sample volume, initial concentration (12.5, 11.5 and 12.5 mmol/L) and pH = 4.5, 4.6 and 4.9 for Cu(II), Ni(II) and Pb(II) ions, respectively. The effect of chemically modified graphene oxide 4-aminoantipyrine-GO dosage on the adsorption capacity is investigated in the range 0.01–0.05 g, and the results is presented graphically in Fig. 7a, which clears that the adsorption capacity qe decreases from 2.5 to 1.05, 2.125 to 0.825 and 2.625 to 1.2 mmol/g with the increasing in adsorbent mass from 0.01 to 0.05 g for Pb(II), Ni(II) and Cu(II) ions, respectively. While the percent of removal increases with adsorbent dose from 0.01 to 0.05 g, that is showed in Fig. 7b from 8% to 16.8%, 7.39% to 14.347% and 8.4% to 19.2% for Pb(II), Ni(II) and Cu(II) ions, respectively. Although the percentage adsorption increases with adsorbent dose, the amount of metal ion adsorbed per unit mass decreases because it is related to the unsaturation of adsorption sites through the adsorption process and the interactions between the particles, as aggregation producing from high adsorbent concentration. This aggregation leads to a decrease in the total surface area of the adsorbent [55].

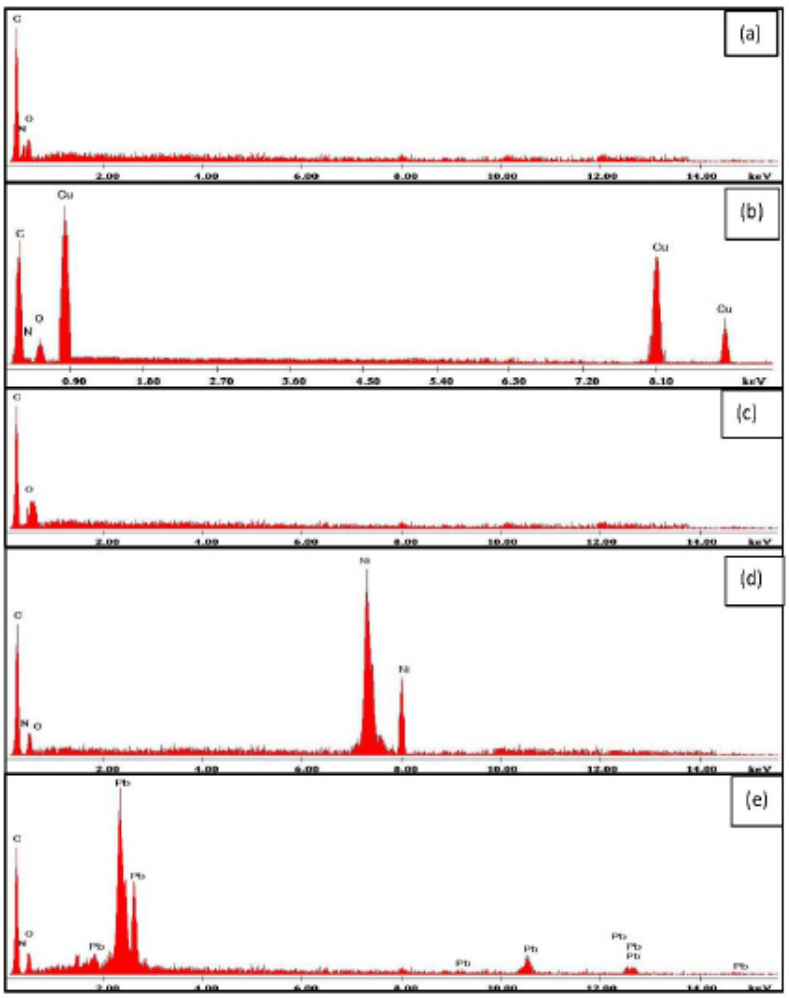

Fig. 5. EDX of a) GO, b) 4-aminoantipyrine-GO, c) 4-aminoantipyrine-GO-pb^{+2}, d) 4-aminoantipyrine-GO-Cu^{+2}&e) 4-aminoantipyrine-GO-Ni^{+2}.

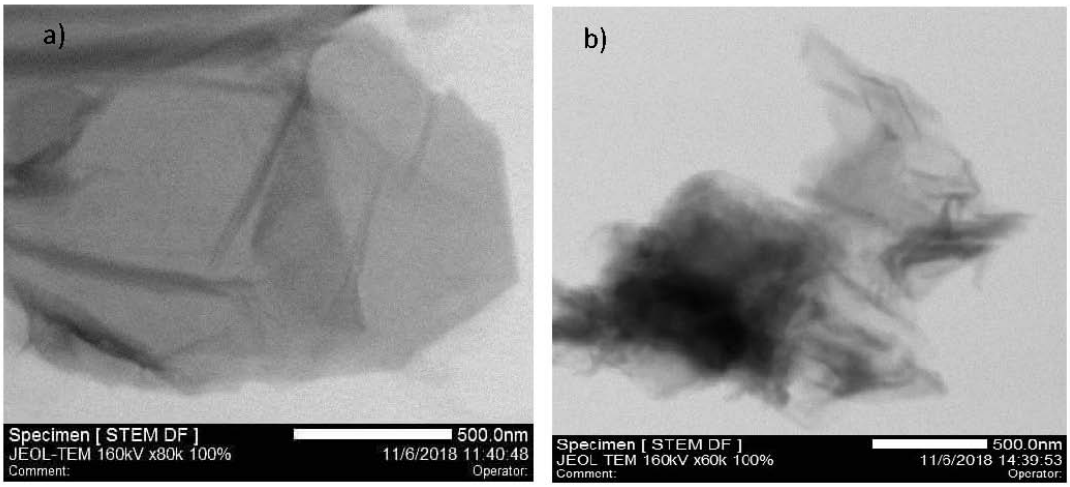

Fig. 6. TEM images of a)GO&b) 4-aminoantipyrine-GO.

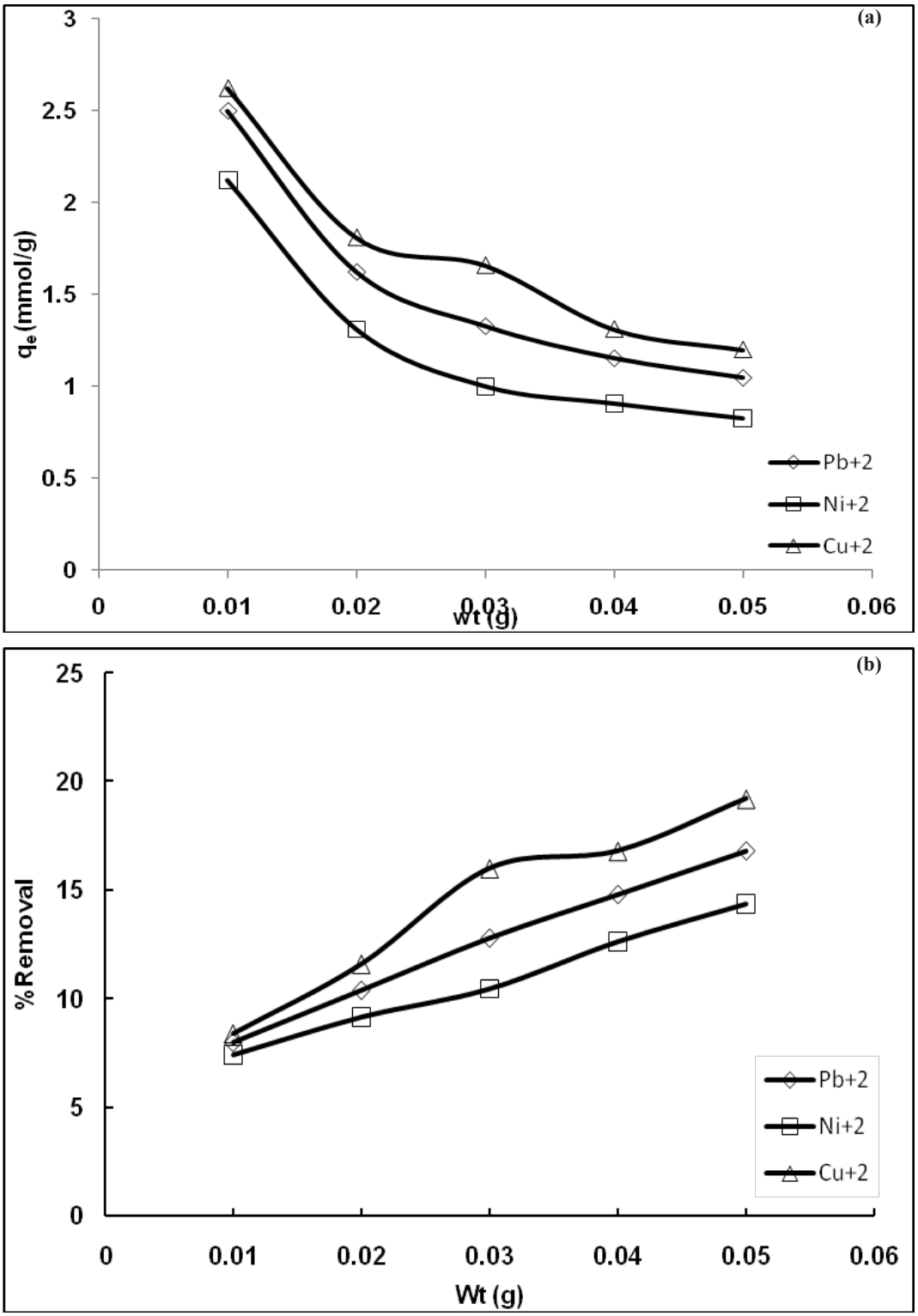

Fig. 7. Effect of 4-aminoantipyrine-GO dosage on, a) The adsorption capacity & b) The percent of removal, towards Cu(II), Ni(II) and Pb(II) ions (Conditions:C_o = 0.0125, 0.0115 & 0.0125 mol/L, T = 303 K, V = 25 ml, t = 2h,pH = 4.5, 4.6 and 4.9).

Effect of pH

The effect of initial pH on the adsorption of Cu(II), Ni(II) and Pb(II) by chemically modified graphene oxide (4-aminoantipyrine-GO) was studied by varying pH over the range of 2.5 to 6.5 using 0.1 N NaOH/HCl. The nitrogen atom of the amide group of 4-aminoantipyrine chelating ligands can bind a metal ion by electron pair-sharing to form a metal chelate-complex. The effect of pH on the removal of Cu(II), Ni(II) and Pb(II) by (4-aminoantipyrine-GO) nanosheets is showed in Fig. 8, where the adsorption capacity increases by the increasing in pH to reaching the maximum adsorption capacity qe (4.00, 3.75 and 3.50 mmol/g) at pH 5.5, 5.35 and 5.9 for Cu(II), Pb(II) and Ni(II), respectively. Under highly acidic conditions, the (4-aminoantipyrine-GO) was less sorption of the metal ion because the binding sites for metal ions onto the adsorbent are occupied by H_3O^+ ions which restrict the approach of Cu(II), Ni(II) and Pb(II) cations as a result repulsive forces [56,57]. However, as the pH value of the solution increases, a number of associated H_3O^+ ions is diminished, exposing an increasing in negatively charged adsorbent surface and thereby allowing an increasing number of positively charged metal ions to be adsorbed. After reaching the maximum adsorption capacity q_e, no further adsorption occurred due to the precipitation of metal ions as metal hydroxide [58].

Effect of initial ion concentration

The effect of the initial concentration on the removal of Cu(II), Pb(II) and Ni(II)ions using (4-aminoantipyrine-GO) at the optimum pH = 5.5, 5.35 and 5.9, respectively, at room temperature 30 ^oC and 0.01 g of adsorbent are shown in Fig. 9. The results indicate that the equilibrium sorption capacities of the sorbent increase with increasing the initial Cu(II), Pb(II) and Ni(II) ion concentration due to the strong driving force of the concentration gradient at solid-liquid interface which causes an increase of the amount of metal ions adsorbed on the adsorbent. The dependence of the adsorption capacity of 4-aminoantipyrine-GO on the initial concentration of metal ions was studied by increasing the intial concentration of Cu(II), Ni(II) and Pb(II) ions from 0.9 to 12.5, 1 to 10.5, and 1.05 to 12 mmol/L, respectively. The amount of Cu(II), Ni(II) and Pb(II) ions adsorbed at equilibrium (q_e) increases from 1.50 to 4.00, 0.75 to 3.50, and 1.25 to 3.75 mmol/g, respectively.

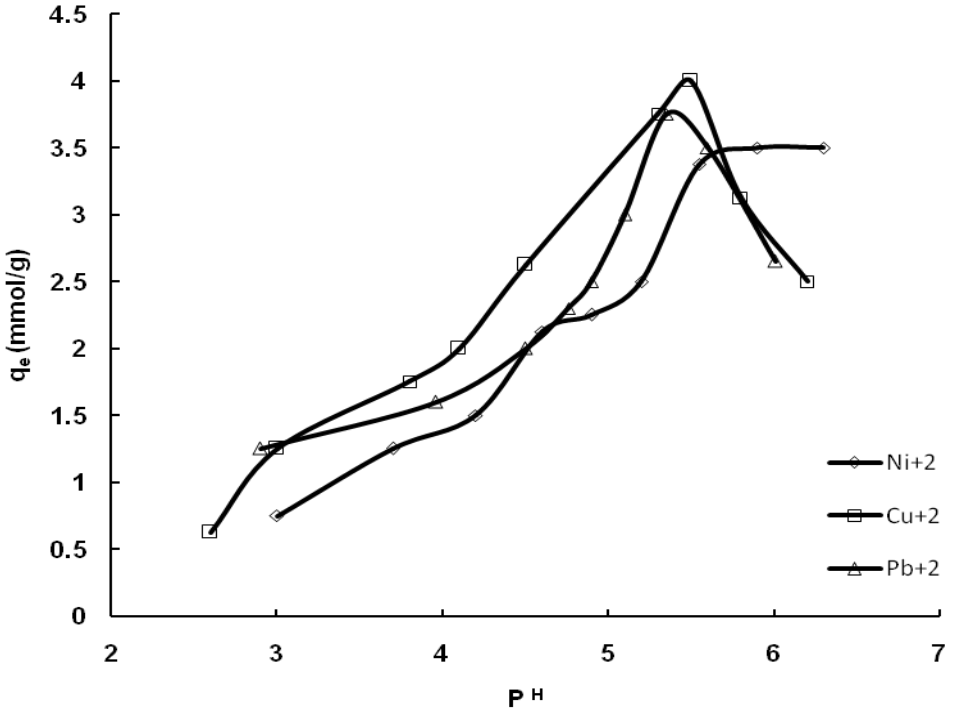

Fig. 8. Effect of pH on The adsorption capacity of (4-aminoantipyrine-GO)nano sheets towards Cu(II), Ni(II) and Pb(II) ions (Conditions:C_o = 0.0125, 0.0105 & 0.012 mol/L, T = 303 K, Adsorbent dose = 0.01 g/25 ml, t = 2h).

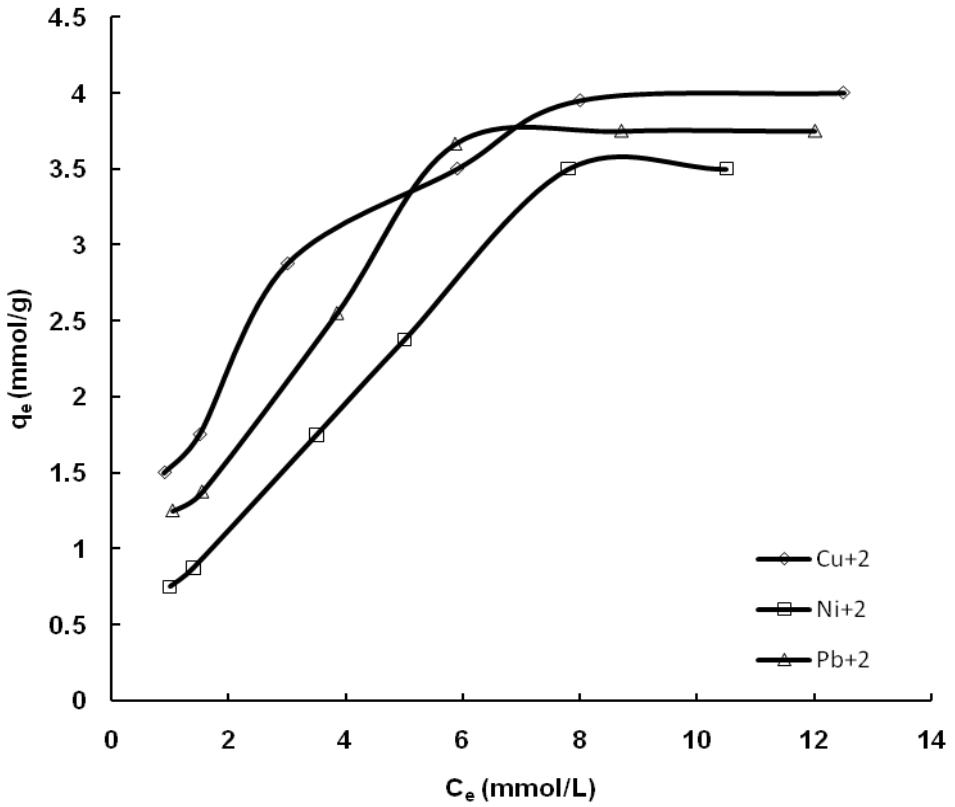

Fig. 9. Effect of initial ion concentration on The adsorption capacity of (4-aminoantipyrine -GO) adsorbent towards Cu(II), Pb(II) and Ni(II) ions (Conditions:pH = 5.5, 5.35 and 5.9, T = 303 K, Adsorbent dose = 0.01 g/25 ml and t = 2h).

Effect of contact time

Figure 10 illustrates the effect of contact time on the adsorption capacity of 4-aminoantipyrine-GOfor the Cu(II), Pb(II) and Ni(II) ions with concentrations of 11.1, 12 and 10.5 mmol/L at pH = 5.5, 5.35 and 5.9, respectively. It is clear that an continuous increase in the adsorption capacity as the time increase until reaching equilibrium between two phases after 6h, q_e= 4.50, 4.375 and 4.20 mmol/g for Cu(II), Pb(II) and Ni(II) ions, respectively.

Effect of temperature

The influence of solution temperature on the adsorption capacity was examined, while other effective parameters were kept constant. The results are shown in Fig. 11, which indicate that the capacity increases by increasing the solution temperature from 30 ^oC to 60 ^oC in steps of 10 ^oC, q_e = 4.950, 4.699 and 4.501 mmol/g at 60 ^oC for Cu(II), Pb(II) and Ni(II) ions, respectively. Generally as the temperature increases the uptake value increases. This behavior may be attributed to: The increase of active site number due to the more flexible 4-aminoantipyrine-GO nano sheets, less dehydration of the active sites and better interactions for the metal ions at elevated temperatures [59]. This enhancing of adsorption also can be attributed to the fact at higher temperatures, cations move faster. This can be due to the fact that the specific or electrostatic interactions become weaker and the ions become smaller, since solvation is reduced [60]. Based on this description, it is clear that the adsorption of Cu(II), Pb(II) and Ni(II) ions on the adsorbent is an endothermic process and this process was a chemical adsorption, confirmed by thermodynamic calculations.

Adsorption isotherms

To optimize the design of an adsorption system to remove heavy metal ions from aqueous solutions, it is important to establish the most appropriate correlation for the equilibration curve. Many adsorption isotherms have been used in this study, Langmuir, Freundlich and Temkin.

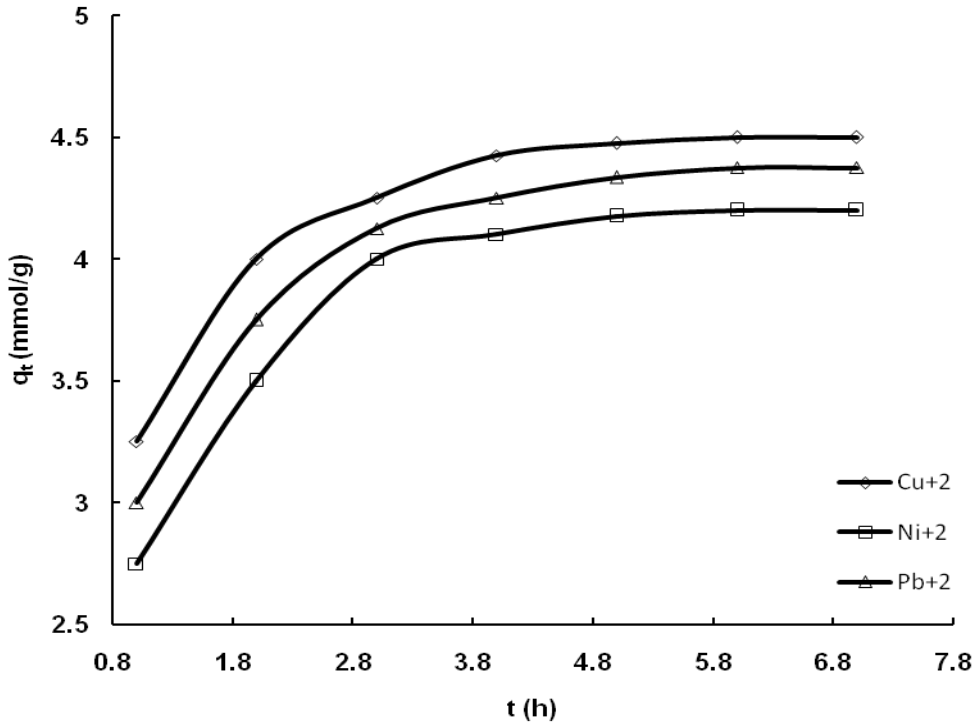

Fig. 10. Effect of contact time on The adsorption capacity of (4-aminoantipyrine-GO) adsorbent towards Cu(II), Pb(II) and Ni(II) ions (Conditions:pH = 5.5, 5.35 and 5.9, C_o = 11.1, 12 and 10.5 mmol/L, T = 303 K, Adsorbent dose = 0.01 g/25 ml).

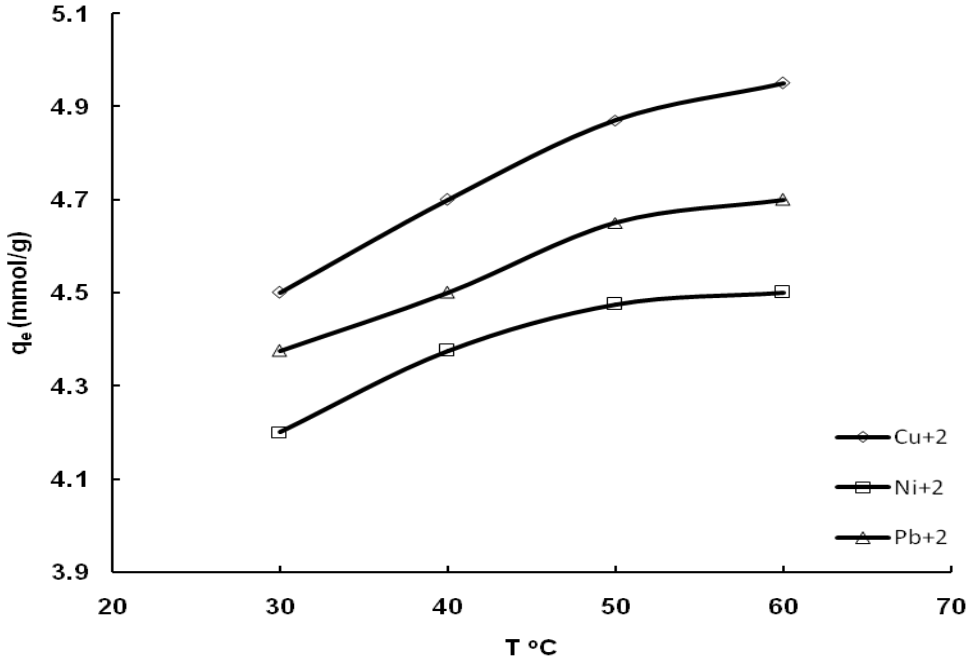

Fig. 11. Effect of Temperature on The adsorption capacity of (4-aminoantipyrine-GO) adsorbent towards Cu(II), Pb(II) and Ni(II) ions (Conditions:pH = 5.5, 5.35 and 5.9, C_o = 11.1, 12 and 10.5 mmol/L, Adsorbent dose = 0.01 g/25 ml, t = 6h).

Langmuir isotherm

The Langmuir adsorption isotherm is based on the homogeneity with monolayer coverage. The isotherm assumes that all sites are equivalent and have uniform surface coverage [61]. The Q^o and b constants are the Langmuir constants related to the adsorption capacity and intensity, respectively. The Langmuir constants Q^o and b are calculated from slope and intercept of linear plot of C_e/q_e versus Ce Fig. 12a and shown in Table 1.

$$C_e/q_e = C_e/Q^o + 1/Q^o b \quad (3)$$

The facility of the adsorption process is determined by the separation factor R_L (Fig. 12b), which is given as

$$R_L = 1/(1+bC_o) \quad (4)$$

The R_L value illustrates an effective interaction between the adsorbent and the adsorbate, when it is between 0 and 1. Values greater than 1 indicate an unfavorable isotherm, and R_L equal to zero determines irreversible isotherm; all the R_L values determined lie between 0 and nearly 0.5 indicating favorable adsorption for Cu(II) and Pb(II) ions on the (4-aminoantipyrine-GO) nanosheets. These properties are summarized in the Langmuir isotherm parameters, and a relatively good regression coefficient (Table 1), indicate effective interaction between the Cu(II) and Pb(II) ions with the (4-aminoantipyrine-GO) nanosheets.

Freundlich isotherm

The Freundlich isotherm [62] yields the constants K_F and n, determining the adsorption capacity and intensity, respectively. The Freundlich adsorption equation can be written as

$$\log q_e = (1/n) \log C_e + \log K_F \quad (5)$$

The Freundlich constants K_F and n are calculated from the slope and intercept of linear plot of log qe versus log Ce (Fig. 13) and shown in Table 1. A favorable adsorption when a Freundlich constant n is between 1 and 10. A higher value of n (smaller value of 1/n) illustrates an effective interaction between the adsorbent and adsorbate. When $1/n < 1$, it corresponds to a normal L-type isotherm, while $1/n > 1$ corresponds to a co-operative sorption [63].

The Temkin isotherm model [64] is based on the indirect interaction between adsorbent and adsorbate. In this isotherm, the extreme values of low and large concentrations are ignored and assumption is made that the adsorption energy for all molecules in form of layer would linearly reduce rather than logarithmically with surface coverage [65]. Temkin model can be expressed as:

$$q_e = B \ln K_T + B \ln C_e \quad (6)$$

Where B and K_T are Temkin constants, which determine the heat of adsorption and equilibrium binding constant, respectively. The values of B and K_T are calculated from the slope and intercept of linear plot of q_e versus ln C_e (Fig. 14) and illustrated in Table 1.

Adsorption kinetics

Lagergren's Pseudo first-order model

The first-order rate expression of Lagergren [66] can be represented mathematically as

$$\log (q_e - q_t) = \log q_{e\,cal.} - (k_1/2.303)\, t \quad (6)$$

Where q_e, and q_t (mmol/g) are the adsorption capacity of metal ion at equilibrium and time t (h), respectively. k_1 is the pseudo first-order rate constant (h^{-1}). This model relates the amount of Cu(II), Pb(II) and Ni(II) adsorbed onto the (4-aminoantipyrine -GO) adsorbent with the rate constants at varying time intervals. The value of the adsorption rate constant k_1 is calculated from slope of the linear plot of log ($q_e - q_t$) versus time (Fig. 15), illustrated in Table 2.

Pseudo second-order model

A pseudo second-order reaction model [67] is used in the study of Cu(II), Pb(II) and Ni(II) adsorption onto the 4-aminoantipyrine-GO adsorbent. It can be represented mathematically as

$$(t/q_t) = (1/k_2 q_{e\,cal}^{\,2}) + (1/q_e)\, t \quad (9)$$

The linear plot of t/q_t versus t for metal ions sorption is illustrated in Fig. 16. The qe (calculated) and the qt (experimental) values are in accordance with the second-order kinetics; these values are 4.54, 4.38, 4.27 mmol/g and 4.50, 4.375, 4.20 mmol/g for Cu(II), Pb(II) and Ni(II) ions, respectively. This symmetry in the values (Table 2) proves the ability of the second-order kinetics for the adsorption data.

Intraparticle diffusion model

The Weber–Morris model isutilized to study the intra-particle diffusion and this relates the amount of metal ions adsorbed to the square root of time [68,69].

$$q_t = K_{id}\ t^{0.5} + C \quad (10)$$

where K_{id} is the intra-particle diffusion constant and q_t is the amount of metal ions adsorbed at time t. A linear plot of q_t versus $t^{0.5}$ with a non-zero intercept (Fig. 17a and 17b) clears that the intraparticle diffusion is not the only rate-limiting step. Also, the Weber–Morris plot does not pass through the origin. It indicates that the boundary layer effect can also influence the kinetics of the adsorption of the metal into the interlayer of the (4-aminoantipyrine-GO) sheets in addition to intraparticle diffusion.

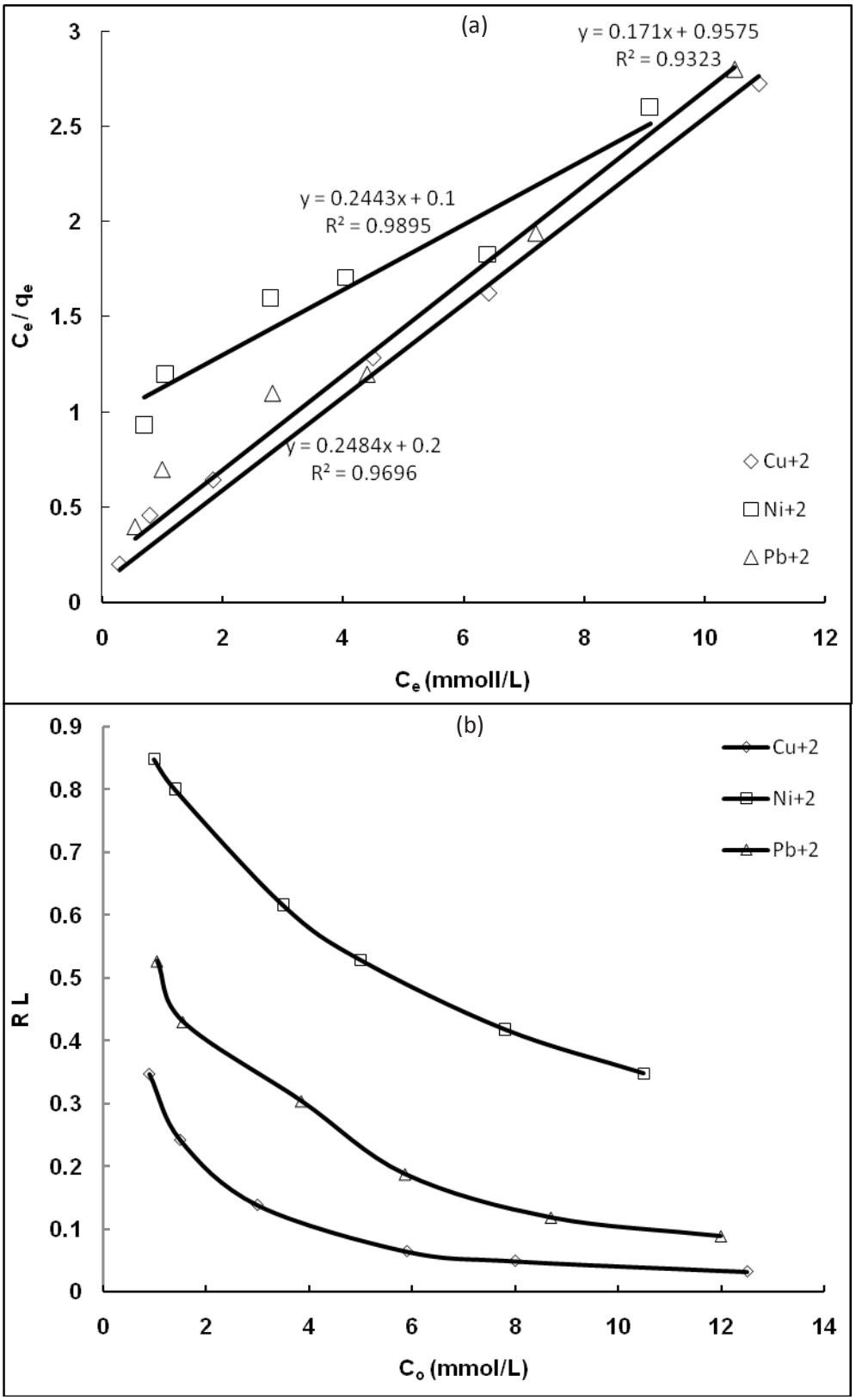

Fig. 12. a) Langmiur adsorption isotherm of Cu(II), Pb(II) and Ni(II) ions & b) variation of separation factor R_L with initial Cu(II), Pb(II) and Ni(II) ions concentrations C_o.

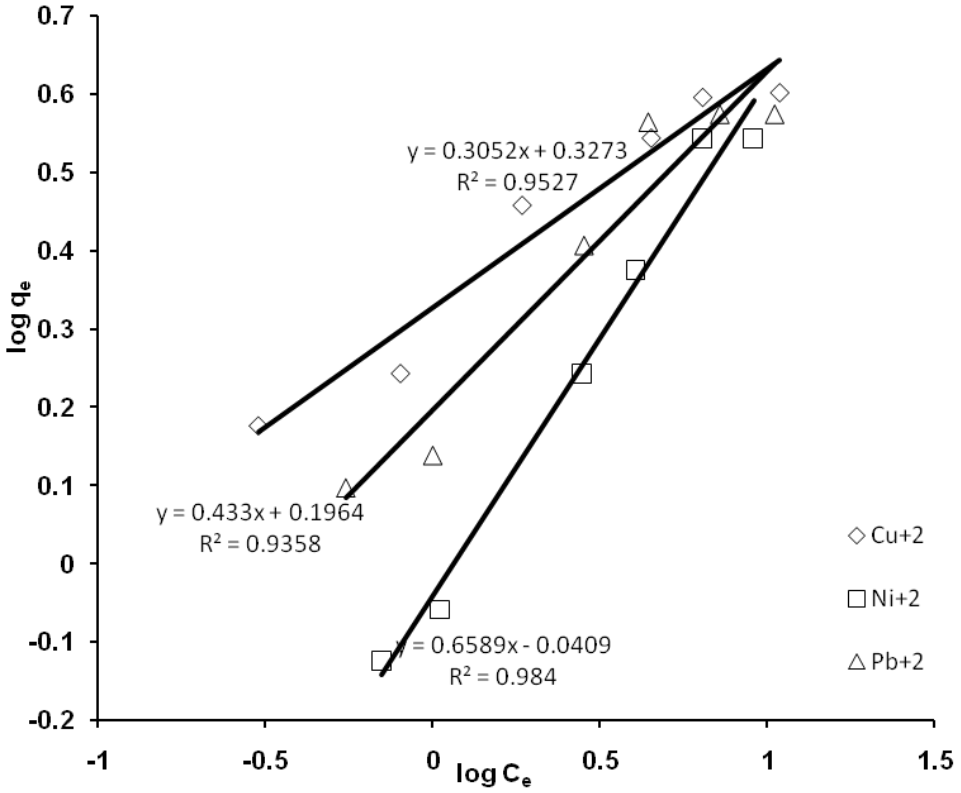

Fig. 13. Freundlich adsorption isotherm of Cu(II), Pb(II) and Ni(II) ions.

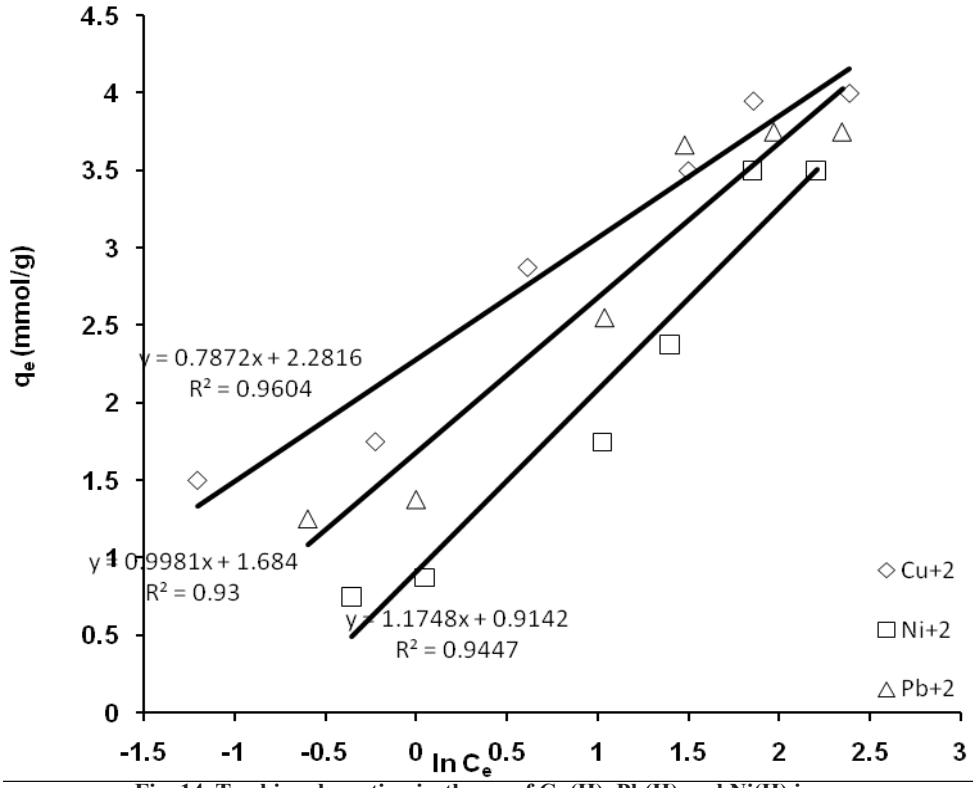

Fig. 14. Temkin adsorption isotherm of Cu(II), Pb(II) and Ni(II) ions.

TABLE 1. The parameters of Langmuir, Freundlich and Temkin isotherms for the removal of Cu(II), Pb(II) and Ni(II) ions using 4-aminoantipyrine -GO at 30°C.

Isotherms	Parameters	Cu^{+2}	Pb^{+2}	Ni^{+2}
Langmuir	Q^o Cal.(mmol/g)	4.100	4.000	5.800
	Q^o Exp.(mmol/g)	4.000	3.750	3.500
	b (L/mmol)	2.440	1.243	0.178
	R^2	0.990	0.970	0.930
Freundlich	K_F (mmol/L)	2.124	1.571	0.910
	(1/n)	0.305	0.433	0.658
	R^2	0.950	0.940	0.980
Temkin	K_T (L/g)	18.135	5.404	2.177
	B (J/mol)	0.7872	0.998	1.170
	R^2	0.960	0.930	0.940

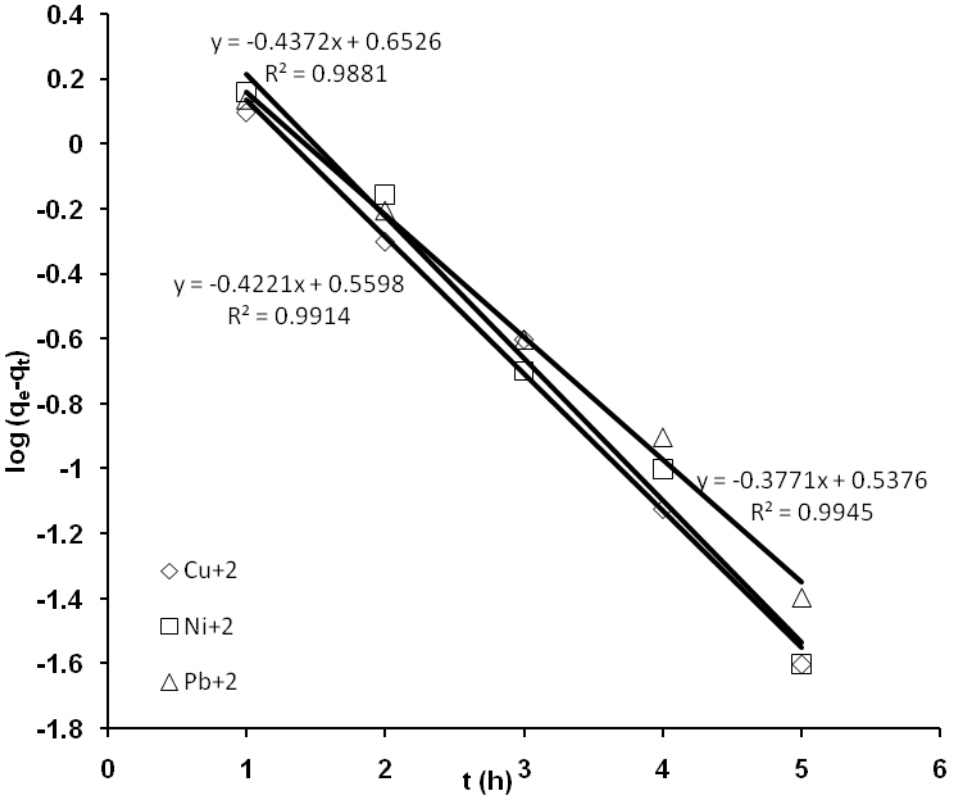

Fig. 15. The first order kinetic plot of Cu(II), Pb(II) and Ni(II) ions onto 4-aminoantipyrine-GO sheets.

TABLE 2. The kinetic parameters for the removal of Cu(II), Pb(II) and Ni(II) ions using 4-aminoantipyrine-GO at 30°C

Kinetic models	Parameters	Cu^{2+}	Pb^{+2}	Ni^{+2}
Pseudo first order	k_1 (h^{-1})	0.824	0.868	1.006
	R^2	0.986	0.994	0.988
	q_e(Calc.) (mmol/g)	0.299	3.440	4.493
Pseudo second order	k_2 (g/ mmol h)	1.936	2.599	1.368
	R^2	0.995	0.990	0.990
	q_e(Calc.)(mmol/g)	4.540	4.380	4.270
	q_e (Exp.) (mmol/g)	4.500	4.375	4.200
Intraparticle diffusion model	K_{id} (mmol $g^{-1}h^{-0.5}$)	1.388	1.550	1.712
	R^2	0.958	0.986	0.990

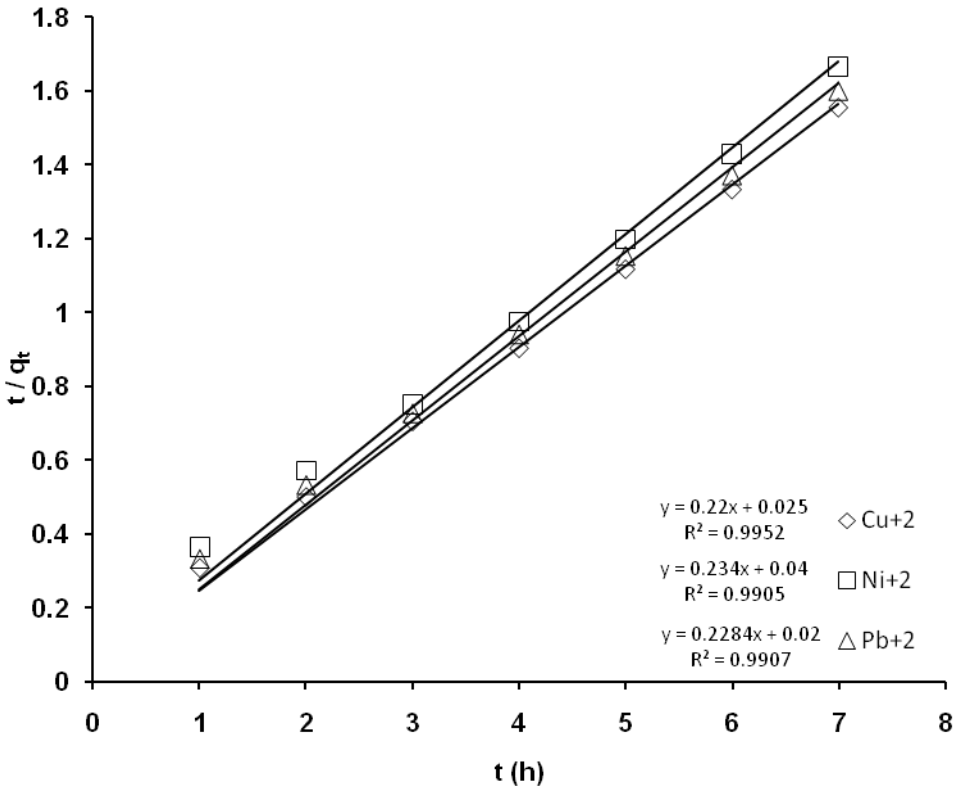

Fig. 16. The second order kinetic plot of Cu(II), Pb(II) and Ni(II) ions onto 4-aminoantipyrine -GO sheets.

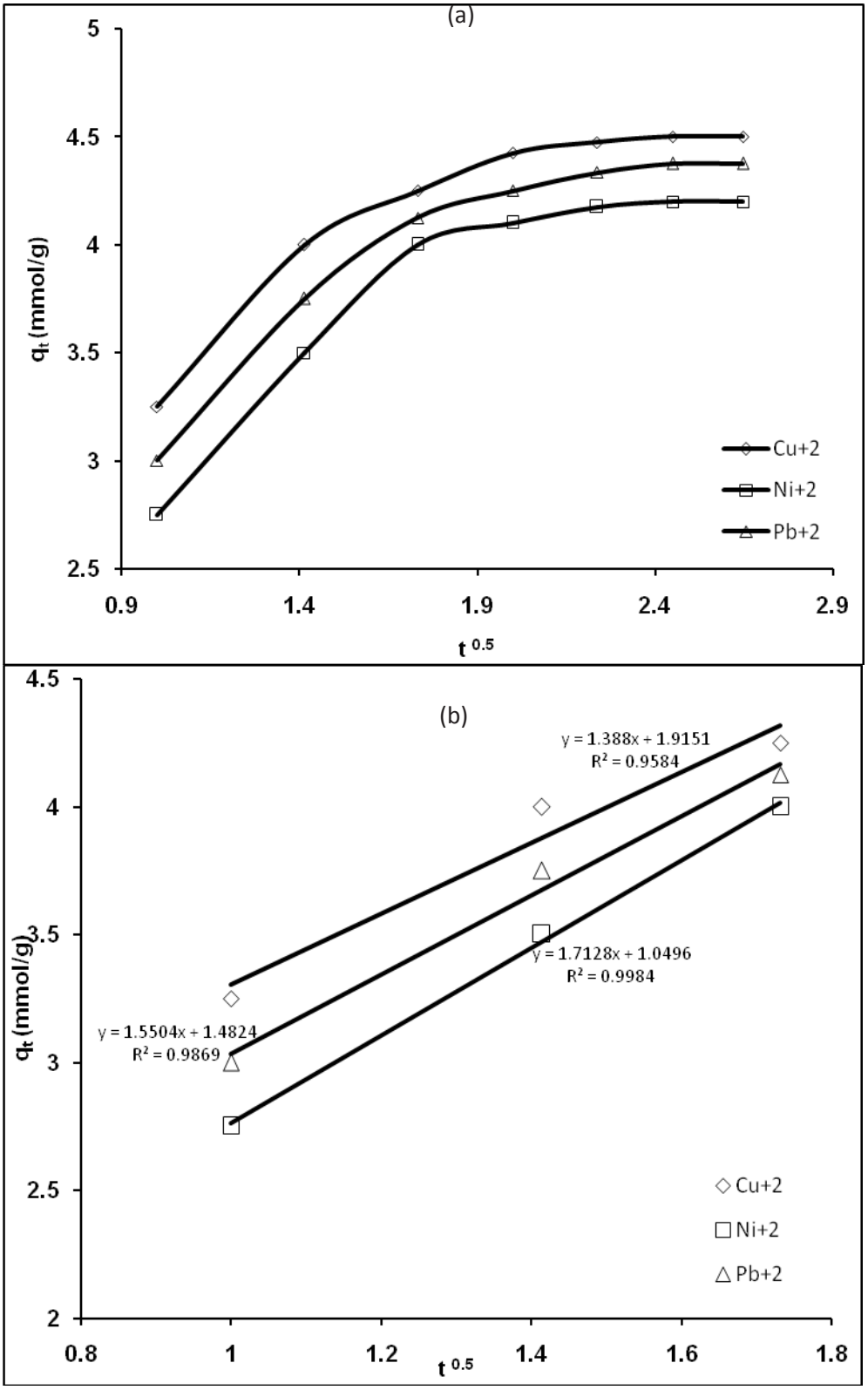

Fig. 17. a) Plot of weber-morris intra particle diffusion model for the adsorption of Cu(II), Pb(II) and Ni(II) ions onto 4-aminoantipyrine -GO sheets & b) Test of the applicability of the intera-particle diffusion model for describing the adsorption of Cu(II), Pb(II) and Ni(II) ions onto 4-aminoantipyrine -GO sheets.

Adsorption thermodynamic parameters

To know the thermodynamic nature of the adsorption process, several adsorption thermodynamic parameters including standard enthalpy (ΔH^O), standard entropy (ΔS^O), and standard Gibbs free energy (ΔG^O) were determined. The amounts of ΔH^O and $\Delta S^O$are calculated from the slope and intercept of the straight line obtained from plotting ln K_d values versus reciprocal temperature (Fig. 18), respectively, and using the following equations [10]:

$$K_d = [(C_o - C_e)V]/[C_e m] \quad (13)$$

$$\ln K_d = (\Delta S^O/R) - (\Delta H^O/RT) \quad (14)$$

Where K_d is distribution coefficient of metal ions on adsorbent C_o and C_e are the initial and final metal ion concentration in the aliquots, respectively. V (ml) is the solution volume and m (g) is the mass of sorbent. ΔH^O, ΔS^O and T are the standard enthalpy standard entropy and temperature in Kelvin, respectively, and R is the gas constant. The standard Gibbs free energy, ΔG^O, of specific adsorption was calculated from the well-known equation [10]:

$$\Delta G^O = -R\ T \ln K_d \quad (15)$$

The positive value of ΔH^O and negative value ΔG^O suggest that the sorption of Cu(II), Pb(II) and Ni(II) ions on (4-aminoantipyrine-GO) is an endothermic and a spontaneous process (Table 3).

The positive value of ΔS^O demonstrates the increasing the randomness at the solid/liquid interface during the adsorption process and thus the decreasing value of ΔG^O with increasing the temperature, indicate that Cu(II), Pb(II) and Ni(II) ions adsorption on the adsorbent is more spontaneous at higher temperatures.

Regeneration and recycling studies

The desorption studies of Cu(II), Pb(II) and Ni(II) ions from the (4-aminoantipyrine-GO) adsorbent show that the Cu(II), Pb(II) and Ni(II) ions were quantitatively desorbed with recovery nearly 98.5%, 97.0% and 90.0% for Ni(II), Pb(II) and Cu(II) ions, respectively, by using 0.1 M HNO_3. The results are shown in Fig. 19. To determine the reuse ability of the 4-aminoantipyrine-GO adsorbent, the effective adsorption-desorption process was carried out for three times at initial concentration of Cu(II), Pb(II) and Ni(II) ions = 1 mmol/L, adsorbent dose 0.05 g and contact time 3 h at room temperature. The results proved that 4-aminoantipyrine-GO adsorbent has sufficient chemical stability over several adsorption-desorption cycles.

Comparison of adsorption behaviour based on literature data

The 4-aminoantipyrine-GO adsorbent was compared in terms of adsorption capacity with some recently reported adsorbents. It clears that, in terms of adsorption capacity, the proposed sorbent compares favorably with other adsorbents and its adsorption capacity is high compared to other adsorbents (Table 4) [70-82].

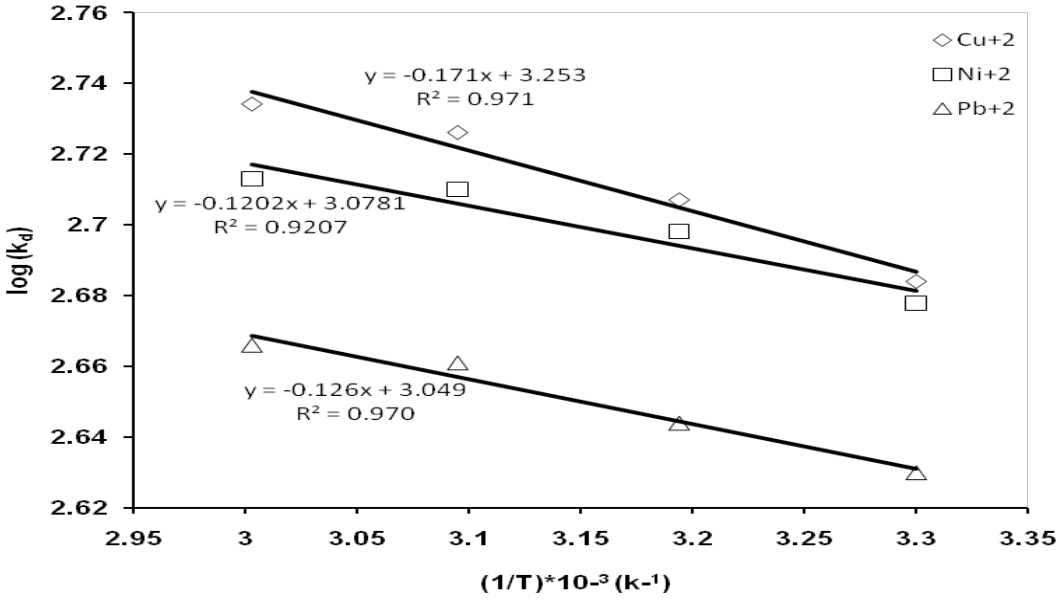

Fig. 18. The effect of temperature on the distribution coefficient of Cu(II), Pb(II) and Ni(II) ions onto 4-aminoantipyrine-GO sheets.

TABLE 3. Thermodynamic parameters for the removal of Cu(II), Pb(II) and Ni(II) ions using 4-aminoantipyrine-GO adsorbent.

Metal ion	$-\Delta G^{O}$ (kJ/mol)				ΔH^{O} (kJ/mol)	ΔS^{O} (KJ/mol.K)
	303°K	313°K	323°K	333°K		
Cu^{2+}					0.032	0.614
	186.0	192.1	198.3	204.4		
	303°K	313°K	323°K	333°K		
Pb^{+2}					0.023	0.575
	174.2	179.9	185.7	191.4		
	303°K	313°K	323°K	333°K		
Ni^{+2}					0.022	0.581
	176.0	181.8	187.6	193.4		

TABLE 4. Comparison of the adsorption capacities of Cu(II), Pb(II) and Ni(II) ions onto various adsorbents.

Metal ion	Adsorbents	Adsorption capacity mmol/g	Ref.
Cu(II)	Chitosan-GLA matrix	2.7	[70]
	Soy protein hollow microspheres (SPMs)	1.81	[71]
	organo-bentonite	0.371	[72]
	GNS/MnO_2	1.62	[77]
	SMGO	0.987	[78]
	4-aminoantipyrine-GO	4.950	This work
Ni(II)	Soy protein hollow microspheres (SPMs)	3.017	[71]
	Oxidized CNTs	0.839	[73]
	Acid treated sphaer-oplea algae	4.15	[74]
	SDS-GO	0.939	[79]
	Graphene/δ-MnO_2	0.793	[80]
	4-aminoantipyrine-GO	4.699	This work
Pb(II)	Soy protein hollow microspheres (SPMs)	1.136	[71]
	Chitosan-iron(III) bio-composite beads	0.56	[75]
	Alginate-melamine hybrid sorbent	1.39	[76]
	GO-mβCD	1.508	[81]
	rGONF	0.588	[82]
	4-aminoantipyrine-GO	4.502	This work

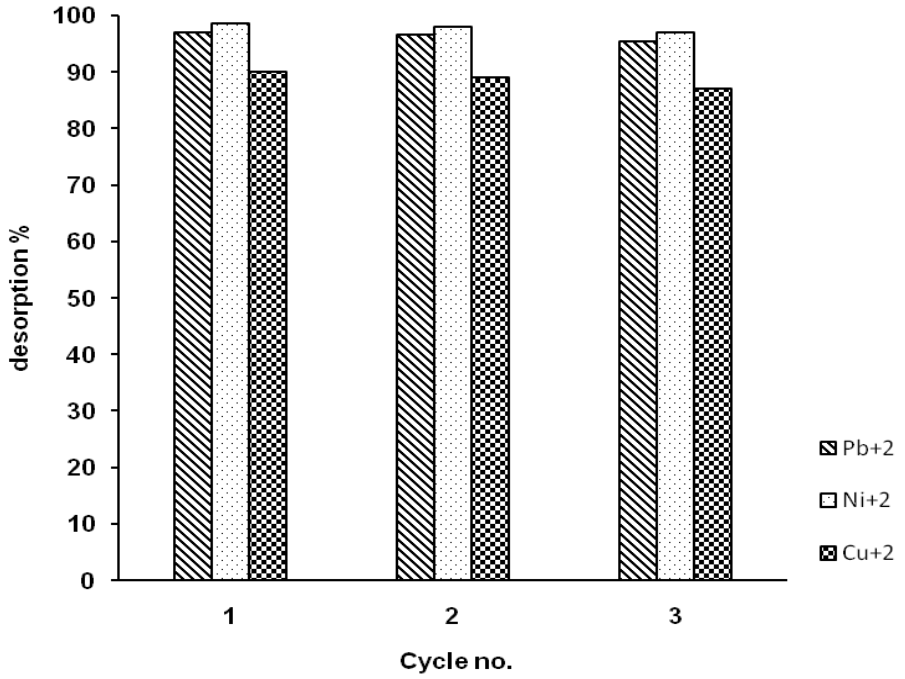

Fig. 19. Recycling of loaded 4-aminoantipyrine -GO adsorbent (desorption condition: 0.1 M HNO_3 and adsorption condition: pH = 5.5, 5.35 and 5.9, initial concentration of Cu(II), Pb(II) and Ni(II) = 1 mmol/L, dose: 0.05 g/25 ml and t = 3h).

Conclusions

The GO, GO-Cl and 4-aminoantipyrine-GO were synthesized and characterized by FT-IR, XRD, SEM, EDX, TEM, and Raman spectroscopy. Utilization of the obtained 4-aminoantipyrine-GO nanosheets was for removal of Cu(II), Pb(II) and Ni(II) ions from aqueous solution by batch experiments. The results show that the adsorbent dose, pH of the solution, initial concentration, contact time and temperature significantly affect the adsorption capacity of Cu(II), Pb(II) and Ni(II) ions. The maximum adsorption capacity at the optimum conditions were 4.950, 4.502 and 4.699 mmol/g for Cu(II), Ni(II) and Pb(II) ions, respectively. 4-aminoantipyrine-GO nanosheets were more sensitive for Cu(II) ions than Pb(II) and Ni(II) ions.

The Langmuir and Freundlich adsorption models were used to provide a mathematical description of the adsorption equilibrium of Cu(II), Pb(II) and Ni(II) ions onto 4-aminoantipyrine-GO nanosheets. The results obtained clear that the adsorption equilibrium data are well fitted by the Langmuir model for Cu(II), Pb(II) ions and Freundlich model for Ni(II) ions over the concentration range studied. Pseudo-first order, pseudo-second order and intra-particle diffusion parameters were calculated and it illustrates that the sorption behavior of Cu(II), Pb(II) and Ni(II) ions onto 4-aminoantipyrine-GO nanosheets obeys the second-order kinetics.

Application of standard thermodynamic equations allowed the values of ΔG^O, ΔH^O and ΔS^O for the adsorption process to be determined. Negative values obtained for ΔG^Oindicates the spontaneous nature of the adsorption process. Positive value obtained for ΔH^Oindicates that the adsorption process was endothermic. The positive values obtained for ΔS^O demonstrates the increasing randomness at the solid/ solution interface during the adsorption of Cu(II), Pb(II) and Ni(II) ions onto 4-aminoantipyrine-GO nanosheets. The regeneration and recycling studies show that the sorbent can be regenerated in diluted HNO3 solution. It was found 98.5% of Ni(II), 97.0% of Pb(II) and 90.0% of Cu(II) ions removed from loaded 4-aminoantipyrine-GO in acidic solution.

References

1. Ahmad M., ManzoorK., Venkatachalam P. and Ikram S., Kinetic and thermodynamic evaluation of adsorption of Cu(II) by thiosemicarbazide chitosan, *International J. Biological Macromolecules*, **92**, 910-919 (2016).
2. Lingamdinne L., Koduru J., Choi Y.-L., Chang Y.-Y. and Yang J.-K., Studies on removal of Pb(II) and Cr(III) using graphene oxide based inverse spinel nickel ferrite nano-composite as sorbent, *J. Hydrometallurgy*, **165**, 64–72 (2016).
3. Wu S., Kong L. and, Liu J., Removal of mercury and fluoride from aqueous solutions by three-dimensional reduced-graphene oxide aerogel, *Research on Chemical Intermediates,* **42**, 4513–4530 (2015).
4. Wang H., Yuan X., Wu Y., Huang H., Zeng G., Liu Y., Wang X., Lin N. and Qi Y., Adsorption characteristics and behaviors of graphene oxide for Zn(II) removal from aqueous solution, *J. Applied Surface Science,* **279**, 432–440 (2013).
5. Ostroski I., Barros M., Silva E., Dantas J., Arroyo P. and Lima O., A comparative study for the ion exchange of Fe(III) and Zn(II) on zeolite Nay, *J. Hazard Materials*, **161**, 1404–1412 (2009).
6. Ferreira L., Rodrigues M., de Carvalho J., Lodi A., Finocchio E., Perego P. and Converti A., Adsorption of Ni^{2+}, Zn^{2+} and Pb^{2+} onto dry biomass of Arthrospira (Spirulina) platensis and Chlorella vulgaris. I. Single metal systems, *J. Chemical Engineering,* **173**, 326–333 (2011).
7. Lu C. and Chiu H., Chemical modification of multiwalled carbon nanotubes for sorption of Zn, *J. Chemical Engineering*, **139**, 462–468 (2008).
8. Erturk U., Yerlikaya C. and Sivritepe N., In vitro Phytoextraction Capacity of Blackberry for Copper and Zinc, *Asian J. Chemistry*, **19**, 2161-2168 (2007).
9. Jiang T., Liu W., MaoY., Zhang L., Cheng J., Gong M., Zhao H., Dai L., Zhang S. and Zhao Q., Adsorption behavior of copper ions from aqueous solution onto graphene oxide–CdS composite, *J. Chemical Engineering,* **259**, 603–610 (2015).
10. Pan M., Wu G., Liu C., Lin X. and Huang X., Enhanced Adsorption of Zn(II) onto Graphene OxidesInvestigated Using Batch and Modeling Techniques, *J. Nanomaterials*, **8**, 806 (2018).
11. Di Natale F., Lancia A., Molino A., Di Natale A. M., Karatza D. and Musmarra D., Capture of mercury ions by natural and industrial materials, *J. Hazard Materials*, **132** 220–225 (2006).
12. Li G., Zhao Z., Liu J. and Jiang G., Effective heavy metal removal from aqueous systems by thiol functionalized magnetic mesoporous silica, *J. Hazard Materials*, **192**, 277–283(2011).
13. Di Natale F., Erto A., Lancia A. and Musmarra D., A procedure to design a permeable Adsorptive Barrier (PAB) for contaminated groundwater remediation, *J. Hazard Materials,* **192**, 1842–1850 (2011).
14. Xiang B., Ling D., Lou H. and Gu H., 3D hierarchical flower like nickel ferrite/manganese dioxide toward lead (II) removal from aqueous water, *J. Hazard Materials*, **325**, 178–188 (2017).
15. Pinheiro P., Tavares D., Daniel-da-Silva A., Lopes C., Pereira E., Arau´jo J., Sousa C. and Trindade T., Ferromagnetic Sorbents Based on Nickel Nanowires for Efficient Uptake of Mercury from Water, *J. ACS Applied Materials & Interfaces*, **6**, 8274–8280 (2014).
16. Shukla S., Pai R.and Shendarkar A., Adsorption of Ni(II), Zn(II) and Fe(II) on modified coir fibres, *J. Separation Purification Technology,* **47**, 141–147 (2006).
17. Pramanik S., Dhara P. and padhyay P., A chelating resin containing bis(2-benzimidazolymethyl) amine: synthesis and metal-ion uptake properties suitable for analytical application, *J. Talanta*, **63**, 485–490 (2004).
18. Cao Q., Y. Liu, C. Wang and J. Cheng, Phosphorus-modified poly (styrene-co-divinylbenzene) PAMAM chelating resin for the adsorption of uranium(VI) in aqueous, *J. Hazard Materials*, **263**, 311–321(2013).
19. Qu R., Sun C., Wang C., Ji C., Cheng G., Wang X. and Xu G., Syntheses and adsorption properties for Hg^{2+} of chelating resin of crosslinked polystyrene-supported 2,5-dimercapto-1,3,4-thiodiazole, *J. Applied Polymer Science,* **92**, 1646–1652 (2004).
20. Kabiri S., Tran D., Azari S. and Losic D., Graphene-Diatom Silica Aerogels for Efficient Removal of Mercury Ions from Water, *J. ACS Applied Materials & Interfaces*, **7,** 11815–11823 (2015).

21. Theron J., Walker J. and Cloete T., Nanotechnology and water treatment: applications and emerging opportunities, *J. Critical Reviews in Microbiology*, **34**, 43–69 (2008).

22. Peng W., Li H., Liu Y. and Song S., A review on heavy metal ions adsorption from water by graphene oxide and its composites, *J. Molecular Liquids,* **230**, 496–504 (2017).

23. SunY., Li J.and WangX., The retention of uranium and europium onto sepiolite investigated by macroscopic, spectroscopic and modeling techniques, *J. Geochimaet Cosmochima, Acta*, **140**, 621–643(2014).

24. Sun Y., Wang X., Ai Y., Yu Z., Huang W., Chen C., Hayat T., Alsaedi A. and Wang X., Interaction of sulfonated graphene oxide with U(VI) studied by spectroscopic analysis and theoretical calculations, *J. Chemical Engineering,* **310**, 292–299 (2017).

25. Tang J., Huang Y., Gong Y., Lyu H., Wang Q. and Ma J., Preparation of a novel graphene oxide/ Fe-Mn composite and its application for aqueous Hg(II) removal, *J. Hazard Materials,* **316**, 151–158(2016).

26. Zhang Y., Zhang S., Gao J. and Chung T.-S, Layer-by-layer construction of graphene oxide (GO) framework composite membranes for highly efficient heavy metal removal, *J. Membrane Science.*, **515**, 230–237 (2016).

27. Tan P., BiQ., Hu Y., Fang Z. and Chen Y., Cheng J., Effect of the degree of oxidation and defects of graphene oxide on adsorption of Cu^{2+} from aqueous solution, *J. Applied Surface Science,* **423**, 1141–1151 (2017).

28. Wan S., He F., Wu J., Wan W., Gu Y. and Gao B., Rapid and highly selective removal of lead from water using graphene oxide-hydrated manganese oxide nanocomposites, *J. Hazard Materials*, **314**, 32–40 (2016).

29. Yari M., Rajabi M., Moradi O., Yari A., Asif M., Agarwal S. and Gupta V., Kinetics of the adsorption of Pb(II) ions from aqueous solutions by graphene oxide and thiol functionalized graphene oxide, *J. Molecular Liquids*, **209**, 50–57(2015).

30. Zhang J., Gong J.-L., Zenga G.-M., Ou X.-M., Jiang Y., Chang Y.-N., Guo M., Zhang C. and Liu H.-Y., Simultaneous removal of humic acid/fulvic acid and lead from landfill leachate using magnetic graphene oxide, *J. Applied Surface. Science*, **370**, 335–350 (2016).

31. Sun Y., Shao D., Chen C., Yang S. and Wang X., Highly efficient enrichment of radionuclides on graphene oxide-supported polyaniline, *J. Environmental Science Technology,* **47**, 9904–9910 (2013).

32. Sun Y., Chen C., Tan X., Shao D., Li J., Zhao G., Yang S., Wang Q. and Wang X., Enhanced adsorption of Eu(III) on mesoporous Al_2O_3/ expanded graphite composites investigated by macroscopic and microscopic techniques, *J. Dalton Transaction*, **41**, 13388–13394 (2012).

33. Sun Y., Yang S., Chen Y., Ding C., Cheng W. and Wang X., Adsorption and Desorption of U(VI) on Functionalized Graphene Oxides: A Combined Experimental and Theoretical Study, *J. Environmental Science Technology*, **49**, 4255–4262 (2015).

34. Yang P., Liu Q., Liu J., Zhang H., Li Z., Li R., Liu L. and Wang J., Bovine Serum Albumin-Coated Graphene Oxide for Effective Adsorption of Uranium(VI) from Aqueous Solutions, *J. Industrial Engineering Chemical Research*, **56**, 3588–3598(2017).

35. Russo P., D'Urso L., Hu A., Zhou N. and Compagnini G., In liquid laser treated graphene oxide for dye removal, *J. Applied Surface Science,* **348,** 85–91 (2015).

36. Parmar K. and Murthy Z., Synthesis of acetone reduced graphene oxide/Fe_3O_4 composite through simple and efficient chemical reduction of exfoliated graphene oxide for removal of dye from aqueous solution, *J. Materials. Science,* **49**, 6772–6783 (2014).

37. Peng Y. and Li J., Ammonia adsorption on graphene and graphene oxide: a first-principles study, *J. Frontiers. Environmental Science & Engineering*, **7**, 403–411 (2013).

38. Zare-Dorabei R., Rahimi R., Koohi A. and Zargari S., Preparation and characterization of a novel tetrakis (4-hydroxyphenyl)porphyrin–graphene oxide nanocomposite and application in an optical sensor and determination of mercury ions. *J. RSC Advances*, **5**, 93310–93317 (2015).

39. Shih Y.-C., Ke C.-Y., Yu C.-J., Lu C.-Y. and Tseng W.-L., Combined Tween 20-stabilized gold nanoparticles and reduced graphite oxide–Fe_3O_4 nanoparticle composites for rapid and efficient

removal of mercury species from a complex matrix. *J. ACS Applied Materials & Interfaces,* **6**, 17437–17445 (2014).

40. Tadjarodi A., Ferdowsi S., Zare-Dorabei R. and Barzin A., Highly efficient ultrasonic-assisted removal of Hg (II) ions on graphene oxide modified with 2-pyridinecarboxaldehyde thiosemicarbazone: adsorption isotherms and kinetics studies, *J. Ultrasonics Sonochemistry*, **33**, 118–128 (2016).

41. Ziaei E., Mehdinia A. and Jabbari A., A novel hierarchical nanobiocomposite of graphene oxide–magnetic chitosan grafted with mercapto as a solid phase extraction sorbent for the determination of mercury ions in environmental water samples. *J. Analytical Chima Acta,* **850**, 49–56(2014).

42. Kumar A. and Jiang S.-J., Preparation and characterization of exfoliated graphene oxide–l-cystine as an effective adsorbent of Hg(ii) adsorption, *J. RSC Advances*, **5**, 6294–6304(2015).

43. Ding S.-Y., Dong M., Wang Y.-W., Chen Y.-T., Wang H.-Z., Su C.-Y. and Wang W., Thioether-based fluorescent covalent organic framework for selective detection and facile removal of mercury (II), *J. American Chemical Society*, **138**, 3031–3037 (2016).

44. Marcano D., Kosynkin D., Berlin J., Sinitskii A., Sun Z., Slesarev A., Alemany L., Lu W. and Tour J., Improved synthesis of graphene oxide, *J. ACS Nano*, **4**, 4806–4814 (2010).

45. Hassan H., Abdelsayed V., Khder A., Abou Zeid K., Terner J., El-Shall M., Al-Resayes S. and El-Azhary A., Microwave synthesis of graphene sheets supporting metal nanocrystals in aqueous and organic media, *J. Materials Chemistry,* **19**, 3832–3837 (2009).

46. Abdelsayed V., Moussa S., Hassan H., Aluri J., Collinson M. and El-Shall M., Photothermal Deoxygenation of Graphite Oxide with Laser Excitation in Solution and Graphene-Aided Increase in Water Temperature, *J. Physical Chemistry Letters*, **1**, 2804–2809 (2010).

47. Tang J., Huang Y., Gong Y., Lyu H., Wang Q. and Ma J., Preparation of a novel graphene oxide/Fe-Mn composite and its application for aqueous Hg(II) removal, *J. Hazard. Materials.,* **316**, 151–158 (2016).

48. Raghubanshi H., Ngobeni S., Osikoya S., Shooto N., Dikio C., Naidoo E., Dikio E., Pandey R. and Prakash R., Synthesis of graphene oxide and its application for the adsorption of Pb^{+2} from aqueous solution, *J. Industrial Engineering. Chemistry,* **47**, 169–178 (2017).

49. Jin Z., Sheng J. and Sun Y., Characterization of radioactive cobalt on graphene oxide by macroscopic and spectroscopic techniques, *J. Radioanalytical. Nuclear Chemistry*, **299**, 1979–1986 (2014).

50. Qi Y., Yang M., Xu W., He S. and Men Y., Natural polysaccharides-modified graphene oxide for adsorption of organic dyes from aqueous solutions, *J. Colloid Interface Science*, **486**, 84–96 (2017).

51. Zhu J., Li Y., Chen Y., Wang J., Zhang B., Zhang J. and Blau W., Graphene oxide covalently fictionalized with zinc phthalocyanine for broadband optical limiting, *J. Carbon*, **49**, 1900–1905 (2011).

52. Zhong X., Jin J., Li S., Niu Z., Hu W., Li R. and Ma J., Aryne cycloaddition: highly efficient chemical modification of graphene, *J. Chemical Communications,* **46**, 7340-7342 (2010).

53. Zhao G., Li J., Ren X., Chen C. and Wang X., Few-layered graphene oxide nanosheets as superior sorbents for heavy metal ion pollution management, *J. Environmental Science Technology*, **45**, 10454–10462 (2011).

54. Ding C., Cheng W., Sun Y. and Wang X., Determination of chemical affinity of graphene oxide nanosheets with radionuclides investigated by macroscopic, spectroscopic and modeling techniques, *J. Dalton Transaction,* **43**, 3888–3896 (2014).

55. Wang F., Wang H. and Ma J., Adsorption of cadmium (II) ions from aqueous solution by a new low-cost adsorbent-Bamboo charcoal, *J. Hazard Materials*, **177**, 300–306 (2010).

56. Gode F. and Pehlivan E., A comparative study of two chelating ion-exchange resins for the removal of chromium(III) from aqueous solution, *J. Hazard Materials*, **B100**, 231–243 (2003).

57. Reddy K. and Reddy A., Removal of heavy metal ions using the chelating polymers derived by the condensation of poly(3-hydroxy-4-acetylphenyl methacrylate) with different diamines, *J. Applied Polymer Science*, **88**, 414–421 (2003).

58. Jing X., Liu F., Yang X., Ling P., Li L., Long C. and Li A., Adsorption performances and

mechanisms of the newly synthesized N, N-di(carboxymethyl) dithiocarbamate chelating resin toward divalent heavy metal ions from aqueous media, *J. Hazard Materials*, **167**, 589–596 (2009).

59. Tahir S. and Rauf N., Thermodynamic studies of Ni(II) adsorption onto bentonite from aqueous solution, *J. Chem Thermodynamics.,* **35**, 2003–2009 (2003).

60. Abd El-Latif M. and Elkady M., Equilibrium Isotherms for Harmful Ions Sorption Using Nano Zirconium Vanadate Ion Exchanger, *J. Desalination*, **255**, 21(2010).

61. Zhang C., Sui J., Li J., Tang Y. and Cai W., Efficient removal of heavy metal ions by thiol-functionalized superparamagnetic carbon nanotubes, *J. Chemical Engineering*, **210**, 45–52 (2012).

62. Freundlich H., Over the Adsorption in Solution, *J. Physical Chemistry*, **57**, 385–470 (1906).

63. Santhana A., Kumar K. and Rajesh N., Graphene oxide–aluminium oxyhydroxide interaction and its application for the effective adsorption of fluoride, *J. RSC Advances*, **3** 2697–2709 (2013).

64. Tempkin M. and Pushed V., Kinetics of ammonia synthesis on promoted iron catalyst, *J. Acta Phys. Chim. USSR.,***12**, 327–356 (1940).

65. Aharoni C. and Ungarish M., Kinetics of activated chemisorption. Part 2.—Theoretical models, *J. Chem. Soc. Faraday Trans.*, **73**, 456-464 (1977).

66. Lagergren S., About the Theory of So-Called Adsorption of Soluble Substances, *Kungliga Svenska Vetenskapsakademiens: Handlingar*, **24**, 1–39 (1898).

67. Ho Y., Review of second-order models for adsorption systems, *J. Hazard Materials*, **136**, 681–689 (2006).

68. Wang X., Zhou Y., Jiang Y. and Sun C., Studies on the Adsorption of Methylene Blue Dye from Aqueous Solution onto Low-Cost Tartaric Acid Treated Bagasse, *J. Hazard Materials*, **157**, 374–385 (2008).

69. Weber W. and Morris J., Kinetics of Adsorption of Carbon from Solution, *J. of the Sanitary Engineering Division*, **89** 31–60 (1963).

70. Rabelo R., Vieira R. and Murilo L., Adsorption of Copper(II) and Mercury(II) Ions onto Chemically-modified Chitosan Membranes: Equilibrium and Kinetic Properties, *J. Ads. Sci. & Tech.,* **30**, 1-21(2012).

71. Liu D., Li Z. and Li W., Adsorption Behavior of Heavy Metal Ions from Aqueous Solution by Soy Protein Hollow Microspheres, *J. Industrial & Engineering Chemistry Researcher*, **52**, 11036–11044 (2013).

72. Maramis V., Ayucitra A., Sunarso J. and Ismadji S., Removal of copper ions from aqueous solution by adsorption using LABS-modified bentonite (organo-bentonite), *J. Frontiers of Chemical Science and Engineering,* **6**, 58-66 (2012).

73. Kandah M. and Meunier J., Removal of nickel ions from water by multi-walled carbon nanotubes, *J. Hazard. Materials.,* **146**, 283-8 (2007).

74. Rao P., Kalyani S., Reddy K. and Krishnaiah A., Comparison of Biosorption of Nickel (II) and Copper (II) Ions from Aqueous Solution by Sphaeroplea Algae and Acid Treated Sphaeroplea Algae, *J. Separation Science & Technology*, **40**, 3149-3165 (2005).

75. Lapo B., Demey H., Zapata J., Romero C. and Sastre A., Sorption of Hg(II) and Pb(II) Ions on Chitosan-Iron(III) from Aqueous Solutions: Single and Binary Systems. *J. Polymer*, **10**, 376-394 (2018).

76. Li K., Wu G., Wang M., Zhou X. and Wang Z., Efficient Removal of Lead Ions from Water by a Low-Cost Alginate-Melamine Hybrid Sorbent. *J. Applied. Science.* **8,** 1518-1530 (2018).

77. Ren Y., Yan N., Feng J., Ma J., Wen Q., Li N. and Dong Q., Adsorption mechanism of copper and lead ions onto graphene nanosheet/δ-MnO_2. *J. Materials Chemistry & Physics,* **136** 538-544 (2012).

78. Hu X.-J., Liu Y.-G., Wang H., Chen A.-W., Zeng G.-M., Liu S.-M., Guo Y.-M., Hu X., LiT.-T., Wang Y.-Q., Zhou L. and Liu S.-H., Removal of Cu(II) ions from aqueous solution using sulfonated magnetic graphene oxide composite. *J. Separation & Purification Technology,* **108**, 189-195 (2013).

79. Salihi E., Wang J., Coleman D. and Šiller L., Enhanced removal of nickel(II) ions from aqueous solutions by SDS-functionalized graphene oxide. *J. Separation Science and Technology*, **51**, 1317 (2016).

80. Ren Y., Yan N., Wen Q., Fan Z., Wei T., Zhang M. and Ma J., graphene/δ-MnO_2 composite as adsorbent for the removal of nickel ions from wastewater. *J. Chemical Engineering*, **175**, 1-7 (2011).

81. Nyairo W., Eker Y., Chrispin K. and Ongeri D., Efficient removal of lead (II) ions from aqueous solutions using methyl-β-cyclodextrin modified graphene oxide. *J. Water Air & Soil Pollution*, **11**, 228 (2017).

82. Lingamdinne L., Kim I.-S., Ha J. and Yang J.-K., Enhanced Adsorption Removal of Pb(II) and Cr(III) by Using Nickel Ferrite-Reduced Graphene Oxide Nanocomposite. *J. Metals-Open Acc. Metallurgy*, **7**, 225 (2017).

اكسيد الجرافين الجديد المعدل لازالة الايونات الثنائية للنحاس و الرصاص و النيكل من المحاليل المائية

عبد الفتاح فاضل شعبان[1]، احمد عبد السلام خليل[1]، بوسى سامى عليوة[2]، محمد نادر اسماعيل[3] و اسامة محمد الدمرداش[2]

[1]قسم الكيمياء - كلية العلوم - جامعة بنها - بنها - مصر.

[2]قسم العلوم اساسية - كلية الهندسة ببنها - جامعة بنها - مصر.

[3]قسم البلمرات والمخضبات - المركز القومى للبحوث - الدقى - الجيزة - مصر.

هذه الطريقة الفعالة لإزالة أيونات الرصاص (II) والنحاس (II) والنيكل (II) من المحاليل المائية ، تعتمد على تطوير أكسيد الجرافين المعدل الجديد ، من خلال التفاعل بين أكسيد الجرافين و(-4أمينو أنتيبيرين). وتم توصيف المركب بشكل كامل عن طريق التحاليل الطيفية المختلفة مثل FT-IR و XRD و SEM و EDX و TEM والرامن. تم تحضير أكسيد الجرافين باستخدام طريقة همرز المعدلة عن طريق تفاعل برمنجنات البوتاسيوم مع الجرافيت في وجود مزيج من أحماض الكبريتيك والفوسفوريك. تم استخدام هذه المركب الصلب ذا الخواص الامتزازية في ازالة أيونات الرصاص والنحاس والنيكل الثنائية من المحاليل المائية بسبب وجود مجموعات الاميد الوظيفية، مما ينتج عنه امتزاز فعال. كما تلعب المجموعات الوظيفية الغنية بالأكسجين على سطح أكسيد الجرافين دورًا مهمًا في امتصاص أيونات المعادن. تم تطبيق نماذج لانجمير و فرندلش و تمكن وجد أن امتزاز ايونات النحاس و النيكل يتبع مسار لانجمير بينما يتبع النيكل مسار فرندلش. كما تم دراسة حركية امتزاز هذه الايونات على سطح اكسيد الجرافين المحسن. تشير نتائج المعاملات الديناميكية الحرارية إلى الامتزاز الكيميائي. تم إعادة استخدام اكسيد الجرافين المحسن بنجاح لثلاث دورات.